The Meteoritical Society

Meteoritics & Planetary Science 49, Nr 4, 473–502 (2014)
doi: 10.1111/maps.12271

Testing variations within the Tagish Lake meteorite—I: Mineralogy and petrology of pristine samples

Alexandra I. BLINOVA[1*], Thomas J. ZEGA[2,3], Christopher D. K. HERD[1], and Rhonda M. STROUD[2]

[1]Department of Earth and Atmospheric Sciences, University of Alberta, 1-23 Earth Sciences Building, Edmonton, Alberta T6G 2E3, Canada
[2]Materials Science and Technology Division, Naval Research Laboratory, 4555 Overlook Ave. SW, Washington, District of Columbia 20375, USA
[3]Present Address: Department of of Planetary Sciences, Lunar and Planetary Laboratory, University of Arizona, 1629 E. University Blvd., Tucson, Arizona 85721–0092, USA
[*]Corresponding author. E-mail: blinova@ualberta.ca

(Received 03 July 2012; revision accepted 27 December 2013)

Abstract–Four samples (TL5b, TL11h, TL11i, and TL11v) from the pristine collection of the Tagish Lake meteorite, an ungrouped C2 chondrite, were studied to characterize and understand its alteration history using EPMA, XRD, and TEM. We determined that samples TL11h and TL11i have a relatively smaller proportion of amorphous silicate material than sample TL5b, which experienced low-temperature hydrous parent-body alteration conditions to preserve this indigenous material. The data suggest that lithic fragments of TL11i experienced higher degrees of aqueous alteration than the rest of the matrix, based on its low porosity and high abundance of coarse- and fine-grained sheet silicates, suggesting that TL11i was present in an area of the parent body where alteration and brecciation were more extensive. We identified a coronal, "flower"-like, microstructure consisting of a fine-grained serpentine core and coarse-grained saponite-serpentine radial arrays, suggesting varied fluid chemistry and crystallization time scales. We also observed pentlandite with different morphologies: an exsolved morphology formed under nebular conditions; a nonexsolved pentlandite along grain boundaries; a "bulls-eye" sulfide morphology and rims around highly altered chondrules that probably formed by multiple precipitation episodes during low-temperature aqueous alteration (≥100 °C) on the parent body. On the basis of petrologic and mineralogic observations, we conclude that the Tagish Lake parent body initially contained a heterogeneous mixture of anhydrous precursor minerals of nebular and presolar origin. These materials were subjected to secondary, nonpervasive parent-body alteration, and the samples studied herein represent different stages of that hydrous alteration, i.e., TL5b (the least altered) < TL11h < TL11i (the most altered). Sample TL11v encompasses the petrologic characteristics of the other three specimens.

INTRODUCTION

On January 18th, 2000, an extremely bright fireball was observed over northern Canada, in the Yukon, Northwest Territories, and British Columbia. This fireball was tracked to an unusual carbonaceous meteorite that fell on the frozen surface of Tagish Lake in British Columbia. The fall was recorded by three local seismic stations; three distant infrasound stations; a U.S. Department of Defense satellite, which observed the entry from the Earth's orbit; and over 90 eyewitnesses (Brown et al. 2002; Hildebrand et al. 2006). Based on all available data from these recordings, it was possible to reconstruct the atmospheric entry model, fragmentation behavior, and size of the fallen body (Hildebrand et al. 2006). It has been estimated that the initial 56 tons of material entered the Earth's atmosphere, but only 1300 kg reached the ground, with 97% of the meteorite

lost to ablation (Brown et al. 2002). This disparity is, in part, due to the unique characteristics of this meteorite, such as high porosity (Brown et al. 2002).

The circumstances of the fall, including the time of the year (subzero ambient temperature) and location (frozen surface of the northern lake), were favorable for recovering several hundred grams of uncontaminated, so-called "pristine," material. Local resident Jim Brook was the first person to discover fragments of the meteorite on the Taku Arm of Tagish Lake on the 25th of January. He was aware of the importance of the meteoritic samples as he was involved with the Geological Survey of Canada collecting snow samples for possible meteoritic dust, so he retrieved the samples with little contamination using plastic bags and stored them frozen, wrapped in aluminum foil, and placed in Ziploc® bags (Hildebrand et al. 2006). Approximately 0.85 kg of pristine samples was collected (Brown et al. 2000). The pristine nature of this material was confirmed by the stepped pyrolysis of "waters" extracted from the bulk sample that bears little terrestrial signature (Baker et al. 2002). Prior to 2006, the pristine samples were on loan to NASA Johnson Space Center, where they were kept under cold, clean conditions. In 2006, a consortium purchase of the pristine material was accomplished (Herd and Herd 2007) yielding approximately 643 g of pristine samples that are currently housed in the Meteorite Collection at the Department of Earth and Atmospheric Sciences, University of Alberta, and 200 g in the Meteorite Collection of the Royal Ontario Museum.

Another set of samples, which are usually referred to as "degraded," were collected by a team in the spring of 2000. These samples were immersed in the lake meltwater and contain evidence of terrestrial contamination confirmed by oxygen isotopes (Russell et al. 2008) and amino acids (Kminek et al. 2002). A total of approximately 5–10 kg samples were recovered during that expedition (Brown et al. 2000). The majority of these samples are now located at the University of Calgary and the University of Western Ontario.

The Tagish Lake meteorite, henceforth referred to as Tagish Lake, is the most friable and unusual meteorite fallen to date. It has a low bulk density of 1.6 g cm^{-3}, extreme porosity of 40%, and it does not fit into the present meteorite taxonomy (Brown et al. 2002). Zolensky et al. (2002) identified two main lithologies (carbonate-poor and carbonate-rich) and a CM1 clast similar to the Kaidun meteorite in the samples that they studied, which included both pristine and degraded specimens. These authors concluded that it is a brecciated meteorite with a matrix-supported mixture of olivine-rich aggregates, rare chondrules, sparse altered CAIs, magnetite, individual grains of olivine, Ca-Fe-Mg-Mn carbonates, and Fe-Ni sulfides. Rare chondrules range in diameter from 0.1 to 1 mm, and rarer CAIs average 2 mm in diameter (Zolensky et al. 2002). Most chondrules and CAIs found by Zolensky et al. (2002) show evidence of aqueous alteration. Olivine and pyroxene compositions are $Fa_{0\text{-}29}$ and $Fs_{1\text{-}7}$, respectively. Matrix consists mostly of intergrown serpentine and saponite.

The latest quantitative bulk mineralogy study of degraded samples (collected in the spring of 2000) by Izawa et al. (2010) determined, through identification of three "new" lithologies (magnetite-, and sulfide-rich, and siderite-dominated), that Tagish Lake is much more varied in major mineralogy than previously thought. In addition, these authors found such minerals as gypsum and talc; however, they were unable to determine whether these minerals are original to the Tagish Lake mineralogy and thus represent a new lithology, or are related to the degraded nature of the examined samples as a result of their terrestrial modification. Izawa et al. (2010) also identified several samples with an increased amount of olivine and magnetite relative to previously characterized Tagish Lake material, but completely lacking in sulfates and have only a minor saponite and serpentine component. They hypothesized that this could be due to the nature of terrestrial melt-water interaction that dissolved sulfates and mechanically separated clay components, or preferentially preserved denser material with less clay components. Although these authors were able to identify new lithologies and noted more mineralogic variation in samples than Zolensky et al. (2002), they have admitted that the disaggregated Tagish Lake material may have undergone mechanical separation and mixing due to melt-water interaction, and may not be linked to any specific lithology. Nevertheless, Izawa et al. (2010) noted that simple mixing of just two lithologies (carbonate-poor and carbonate-rich) identified by Zolensky et al. (2002) cannot explain their newly identified lithologies.

At present, Tagish Lake is classified as C2-ungrouped. There are, however, a few uncertainties and inconsistencies with this classification. The Tagish Lake CAIs found by Zolensky et al. (2002) have a sinuous texture typical of CM chondrites, but the alteration in the former is mostly Mg-rich serpentine, whereas those in the latter tend to contain Fe-rich serpentine (Zolensky et al. 2002). Classification of Tagish Lake is not comprehensive because we know very little about the mineralogic, petrologic, and textural variations. Regardless of the previous work outlined above, little systematic research has been conducted on pristine samples of Tagish Lake (Herd and Herd 2007).

A systematic study of Tagish Lake, most notably on pristine samples, is required to establish a mineralogic framework for determining the variation in the degree of alteration. This in turn will help to identify the least-altered components (e.g., chondrules,

CAIs) as tools for understanding the formation conditions and events that shaped these primitive early solar system objects prior to their incorporation into the Tagish Lake parent body.

This paper is Part I of a project that encompasses the investigation of mineralogic, bulk chemical variations, and isotopic signatures of pristine samples of Tagish Lake available from the University of Alberta Meteorite Collection. Here, we present the results of the detailed mineralogic, petrologic, and textural study of four such samples.

SPECIMENS AND ANALYTICAL METHODS

Four pristine Tagish Lake specimens (TL5b = 0.1739 g; TL11h = 0.272 g; TL11v = two pieces total 0.0746 g; TL11i = 0.3082 g) were chosen on the basis of macroscopic differences seen in a hand sample with the naked eye (e.g., presence/lack of chondrules, grain sizes). Specimen TL5b is a compact, coherent lithology with relatively abundant chondrules or light-colored clasts evident in hand sample. Specimen TL11i is friable, tends to shed a residue of a very fine black dust when handling it, and has been referred to as an example of a "dark, dusty" lithology (Blinova et al. 2009). Sample TL11v is disaggregated pristine material that was collected by Jim Brook and stored in a Ziploc® bag. Macroscopically, sample TL11h is similar to TL11i, and was chosen as a possible second specimen of the "dark, dusty" lithology.

Instruments described below are housed in the Department of Earth and Atmospheric Sciences at the University of Alberta unless indicated otherwise. For microprobe analyses, chips of the above samples (two chips for TL11v, referred as TL11v-1 and TL11v-2) were prepared into 1 inch diameter mounts using Buehler EPOKWICK two part epoxy, and polished on a Logitech WG2 polishing unit with Pellon polishing pads; diamond paste 6, 3, and 1 μm; and Engis OS type 1V lubricant.

Major and minor element concentrations on all samples were obtained by electron probe microanalysis (EPMA) using either a JEOL 8900 Superprobe or a Cameca SX100. Both instruments were operated using a 1–2 μm diameter focused electron beam with a current of 20 nA and an accelerating voltage of 20 kV. Natural minerals such as chromite, albite, diopside, etc. were used as external standards (Jarosewich 2002) for both instruments. The phi-rho-Z correction algorithm was used to correct the electron microprobe data. The instrument calibration was deemed successful when the composition of standards was reproduced within the error margins defined by the counting statistics.

Mineral analyses and bulk rock mineralogy on powdered samples were determined using a Rigaku Ultima IV Powder Diffractometer. Each sample was ground by hand under acetone in an agate mortar and pestle to produce a fine-grained powder. The instrument is equipped with a Co tube and a high-speed Si strip detector. We used Co Kα radiation (λ = 1.7903 Å), a step size of 0.02° 2θ over the range 5–80° 2θ, and 0.3 s count time per step. Samples were top loaded onto the round aluminum holders (or glass where necessary) and spun at 0.5 Hertz. The detection limit for mineral phases is estimated at 1 wt%. Phase identification and semiquantitative phase abundances were determined by Rietveld refinement using the WPF module of JADE 9.0 software from MDI. Rietveld refinement uses nonlinear least-squares optimization to fit the data with a calculated model (calculated as ideal crystals) that is based on powder-diffraction patterns taken from the International Centre for Diffraction Data Powder Diffraction File database (ICDD-PDF). There is a 10% relative error on the calculations made by this method. Most of the samples were found to contain abundant clay minerals, for which no ideal structure model exists in this database, and an amorphous phase.

Three samples (TL5b, TL11i, and TL11h), which represent the range of macroscopic diversity within the pristine Tagish Lake suite, were examined for textural and mineralogic variations in their matrices. We used an FEI Nova 600 focused-ion-beam scanning-electron microscope (FIB-SEM) at the Naval Research Laboratory (NRL) in Washington, D.C., to make electron-transparent cross sections (approximately 10 μm wide) using previously described methods (Zega et al. 2007). A total of four FIB sections were made from polished probe mounts: one each from TL5b and TL11h, and two from TL11i (one from the matrix and one from a lithic clast). All FIB sections were examined at the NRL with a 200 keV JEOL 2200FS transmission electron microscope (TEM) equipped with an energy-dispersive X-ray spectrometer (EDS) and scanning-TEM (STEM)-based bright-field and high-angle annular-dark-field detectors (HAADF). Phase identification was based on mineral structure and chemistry; the former via measurements of high-resolution TEM (HRTEM) images and selected-area electron-diffraction (SAED) patterns, the latter via qualitative EDS.

BULK MINERALOGY

Composition of Major Minerals in the Tagish Lake Meteorite

Minerals such as olivine, pyroxene, carbonate, magnetite, and sulfides represent major minerals and are present in all four samples. Table 1 presents average compositions of these minerals.

Table 1. Average mineral composition in all studied Tagish Lake samples.

	Olivine		Pyroxene (Chond)				Pyroxene (Matrix)		Chromite		Magnetite		Phosphate		Carbonate
	Average	stdev	Average	stdev	Average	stdev	Average	stdev	Average	stdev	Average	stdev	11h	11i	Average
N	20		34		40		11		10		45		23	20	30
wt% oxides															
SiO_2	42.01	0.45	49.07	1.00	59.25	0.85	38.23	0.36	0.49	0.07	0.11	0.14	0.19	0.09	1.26
SO_3	0.01	0.03	—	—	—	—	—	—	—	—	—	—	—	—	—
Na_2O	0.01	0.01	0.11	0.03	0.00	0.01	0.01	0.02	0.00	0.01	0.01	0.05	0.48	0.22	0.10
P_2O_5	0.01	0.02	0.02	0.01	0.00	0.01	0.04	0.02	0.01	0.01	0.00	0.01	39.77		45.92
0.14	0.06														
Fe_2O_3	0.00	0.00	0.00	0.47	0.00	0.09	21.94	0.29	0.69	0.75	68.09	0.76	0.00	0.00	0.00
FeO	2.41	1.90	2.58	0.49	2.45	0.27	0.00	0.00	7.76	0.70	31.01	0.30	1.37	0.11	1.66
Cr_2O_3	0.38	0.22	2.87	0.25	0.70	0.11	0.33	0.01	42.58	3.47	0.05	0.03	0.00	0.01	0.01
MgO	54.50	1.43	18.38	1.62	37.07	0.71	40.23	0.35	18.18	0.66	0.03	0.10	12.25		23.21
1.74	0.16														
K_2O	0.00	0.00	0.00	0.01	0.00	0.01	0.00	0.01	0.01	0.01	0.01	0.02	0.00	0.03	0.01
Al_2O_3	0.12	0.05	8.07	1.22	0.30	0.17	0.15	0.18	28.52	3.93	0.08	0.10	0.05	0.01	0.10
MnO	0.11	0.09	1.14	0.18	0.24	0.09	0.19	0.01	1.82	0.04	0.01	0.02	0.17	0.02	0.03
TiO_2	0.02	0.02	0.87	0.16	0.05	0.02	0.01	0.01	0.41	0.02	0.00	0.01	0.00	0.00	0.00
CaO	0.13	0.02	16.97	1.27	0.26	0.06	0.24	0.14	0.08	0.04	0.04	0.03	30.77	0.01	54.22
NiO	0.02	0.03	0.00	0.01	0.00	0.01	0.06	0.01	0.01	0.01	0.00	0.00	0.03	0.01	0.00
BaO	—	—	—	—	—	—	—	—	—	—	—	—	0.00	0.00	0.03
Total	99.72		100.09		100.31		101.45		100.55		99.48		85.08		69.78

Anions	Based on 4O	Based on 6O			Based on 4O	Based on 32O	Based on 26O			Based on
SiO_2	2.00	3.55	4.00	2.94	0.03	0.09	0.07	0.04	C	1.00
SO_3	0.00	0.00	0.00	0.00	0.00	0.00	0.00	0.00	P	0.00
Na_2O	0.00	0.00	0.00	0.00	0.00	0.00	0.17	0.10		
P_2O_5	0.00	0.00	0.00	0.00	0.00	0.00	6.25	9.27		
FeO (t)	0.05	0.08	0.07	0.71	0.20	31.74	0.42	0.05	Si	0.02
Cr_2O_3	0.01	0.12	0.03	0.02	1.46	0.02	0.00	0.00	Ti	0.00
MgO	1.93	0.99	1.87	2.31	0.78	0.02	6.78			16.51
K_2O	0.00	0.00	0.00	0.00	0.00	0.00	0.00	0.01	Cr	0.00
Al_2O_3	0.00	0.52	0.02	0.01	1.46	0.05	0.01	0.00	Fe	0.06
MnO	0.00	0.04	0.01	0.01	0.04	0.01	0.05	0.01	Mn	0.00
TiO_2	0.00	0.05	0.00	0.00	0.02	0.00	0.00	0.00	Mg	0.08
CaO	0.00	0.66	0.01	0.01	0.00	0.02	12.24	0.01	Ni	0.00
NiO	0.00	0.00	0.00	0.00	0.00	0.00	0.01	0.00	Ca	0.81
BaO	0.00	0.00	0.00	0.00	0.00	0.00	0.00	0.00	Ba	0.00
									Na	0.01
Cations									K	0.00
Si	1.00	1.77	2.01	1.47	0.01	0.03	0.03	0.02		
S	0.00	0.00	0.00	0.00	0.00	0.00	0.34	0.21		
Na	0.00	0.01	0.00	0.00	0.00	0.01	2.50	3.71		
P	0.00	0.00	0.00	0.00	0.00	0.00	0.42	0.05		
Fe^{3+}	0.00	0.00	0.01	0.71	0.02	15.85	0.00	0.00		
Fe^{2+}	0.05	0.08	0.06	0.00	0.19	8.02	0.00	0.00		
Cr	0.01	0.08	0.02	0.01	0.97	0.01	6.78			16.51
Mg	1.93	0.99	1.87	2.31	0.78	0.02	0.00	0.02		
K	0.00	0.00	0.00	0.00	0.00	0.00	0.01	0.00		
Al	0.00	0.34	0.01	0.01	0.97	0.03	0.05	0.01		

				Sulfides							Mesostasis and Other Phases						
stdev	11h[a]	stdev		Average	stdev	Average	stdev	Average	stdev		1[b]	stdev	B&J	2[c]	stdev	3[d]	stdev
	23			73		18		10			14			15		4	
				Troilite		Pentlandite		Pyrrhotite									
1.52	0.03	0.01	S	38.23	0.61	32.73	1.50	36.85	1.91	SiO_2	53.04	1,52	58.70	21.42	4.36	34.79	0.35
—	—	—	Fe	59.08	1.07	31.02	1.19	50.56	4.26	Na_2O	2.87	0.21	7.69	0.19	0.35	0.09	0.02
0.06	0.15	0.08	Ni	2.60	0.77	33.67	1.18	10.64	3.54	P_2O_5	0.04	0.02	—	0.57	0.15	0.14	0.07
	0.11	0.04	0.25	0.13	Co	0.18	0.12	0.90	0.00	0.45	0.13	FeO	2.83	0.52	8.84	10.37	1.35
0.00	0.00	0.00	Cu	0.00	0.00	0.03	0.05	0.01	0.22	Cr_2O_3	0.23	0.05	—	0.40	0.16	0.42	0.06
1.00	7.80	0.75	Zn	0.00	0.02	0.00	0.00	0.01	0.01	MgO	4.97	1.22	0.70	25.22	2.41	2.19	0.96
0.03	0.00	0.00	As	0.06	0.03	0.03	0.04	0.03	0.03	K_2O	0.10	0.02	0.37	0.10	0.06	0.00	0.00
	0.87	1.10	19.54	1.30	Rh	0.00	0.01	0.00	0.01	0.00	0.01	Al_2O_3	23.22	0.95	13.60	17.24	2.12
0.01	0.00	0.01	Pd	0.00	0.01	0.01	0.01	0.01	0.01	MnO	0.71	0.18	0.00	0.22	0.13	25.34	0.48
0.11	0.03	0.01	Ag	0.01	0.01	0.01	0.02	0.01	0.01	TiO_2	0.62	0.12	0.63	0.32	0.10	0.42	0.06
0.04	1.81	0.84	Cd	0.02	0.04	0.00	0.00	0.01	0.02	CaO	11.35	0.41	8.60	0.71	1.24	29.52	0.48
0.00	0.01	0.01	Sn	0.00	0.00	0.00	0.01	0.00	0.00	NiO	0.01	0.01	—	na	na	0.00	0.00
4.92	26.84	1.17	Sb	0.00	0.00	0.01	0.02	0.00	0.00								
0.00	0.01	0.01	Pt	0.00	0.02	0.01	0.02	0.01	0.01								
0.03	0.00	0.00	Au	0.02	0.09	0.00	0.00	0.01	0.03								
	58.40		56.48		Bi	0.00	0.00	0.01	0.04	0.07	0.21						
			Mg	0.00	0.00	0.00	0.00	0.00	0.02								
			Al	0.02	0.01	0.00	0.00	0.02	0.01								
positive charges[e]																	
0.00	1.00	0.00	Si	0.04	0.02	0.04	0.02	0.12	0.17								
0.00	0.003	0.002	Ti	0.00	0.00	0.00	0.00	0.00	0.01								
			Cr	0.05	0.02	0.02	0.02	0.05	0.04								
0.02	0.00	0.00	Total	100.0		97.65		98.48			99.99		99.07	76.75		94.78	
0.00	0.00	0.00															
Al	0.00	0.00	0.00	0.00													
0.00	0.00	0.00															
0.12	0.10	0.01															
0.01	0.02	0.01															
0.15	0.44	0.02															
0.00	0.00	0.00															
0.28	0.43	0.02															
0.00	0.00	0.00															
0.01	0.00	0.00															
0.00	0.00	0.00															

Table 1. *Continued*. Average mineral composition in all studied Tagish Lake samples.

	Olivine		Pyroxene (Chond)				Pyroxene (Matrix)		Chromite		Magnetite				Phosphate
	Average	stdev	Average	stdev	Average	stdev	Average	stdev	Average	stdev	Average	stdev	11h	11i	Average
Fo	97.46														
Fa	2.54														
En			56.3		95.6		76.2								
Fs			6.4		3.89		23.5								
Wo			37.3		0.48		0.32								
Chr									0.49	0.05	0.00	0.00			
Mg									0.01	0.01	1.00	0.00			
Sp									0.49	0.05	0.00	0.00			
Usp									0.02	0.00	0.00	0.00			
Fe^{3+}/Fe^{2+}											1.98	0.03			

[a]Large 11h carbonate enriched in Mn.
[b]Average analyses of 5b chondrule mesostasis in area "a" on Fig. 4c.
[c]Average analyses of 5b chondrule mesostasis in area "b" on Fig. 4d.
[d]Average analyses of Mn-Ca silicate in 11v.
[e]Following Brandelik (2009) CALCMIN calculations.
B&J = Brearley and Jones (1998)—comparative glass analyses for Y-790123 (CM2).

Olivine grains are found both in the chondrules and in the matrix. The majority of olivine compositions in both groups vary between Fo_{99} and Fo_{95}. Isolated olivines in the matrix, which range in size from a few microns up to 400 μm, have compositions of $Fo_{99.4\text{-}99.6}$. Some appear to be fragments. Rare-zoned and oscillatory-zoned olivines were identified in one chondrule in specimen TL11i only. The compositions of the olivines in this chondrule range from Mg-rich cores ($Fo_{98.6\text{-}89.4}$) to Fe-rich rims ($Fo_{66.7\text{-}70.2}$) (Fig. 1a). The majority of olivines, either in chondrules or isolated in the matrix, have well-preserved faceting and appear to have been minimally affected by hydrous alteration.

Similar to olivine grains, pyroxenes are found both in the chondrules and in the matrix. However, unlike olivines, the majority of pyroxenes show a higher degree of hydrous processing. The most common pyroxene composition encountered within the Tagish Lake chondrules is $En_{96}Fs_{3.6}Wo_{0.5}$ and accounts for up to 85% of all pyroxene compositions in these objects. Rare, isolated grains of this composition can also be found in the matrix. The other 15% of pyroxenes in the chondrules are high in Ca, typically $En_{56}Fs_{6.4}Wo_{37.3}$. The majority of the low-Ca pyroxenes in the matrix have the average composition of $En_{76.2}Fs_{23.5}Wo_{0.32}$ (Fig. 1b).

The predominant sulfide composition is pyrrhotite with average Ni content of 2.60 wt%. Some intermediate compositions with average Ni content of 10.64 wt% are also found. Pentlandite contains up to an average of 34 wt% Ni and occurs as exsolutions in pyrrhotite as well as occasional isolated grains (Table 1 and Fig. 2; with data from Zolensky et al. [2002] for comparison).

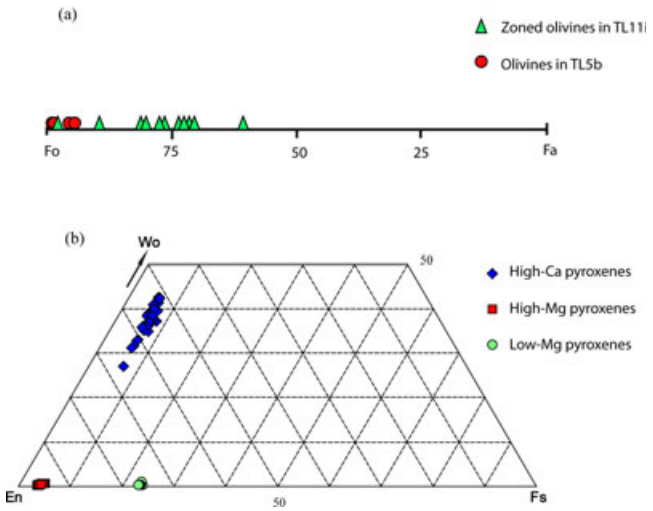

Fig. 1. Compositional diagrams showing (a) the Mg-Fe range of olivine and (b) Mg-Fe-Ca pyroxene compositions in all studied Tagish Lake samples.

Magnetite occurs in all Tagish Lake specimens, but its abundance varies. Our calculations of magnetite based on 32 O atoms showed that its composition is close to the pure magnetite endmember composition with total metal ions of 24 and with Fe^{3+}/Fe^{2+} of 1.988 ± 0.001 (using Droop [1987] for calculation of Fe^{3+} in these and all further analyses). Magnetite morphologies range from platelets to framboids consisting of even smaller framboids. Similar

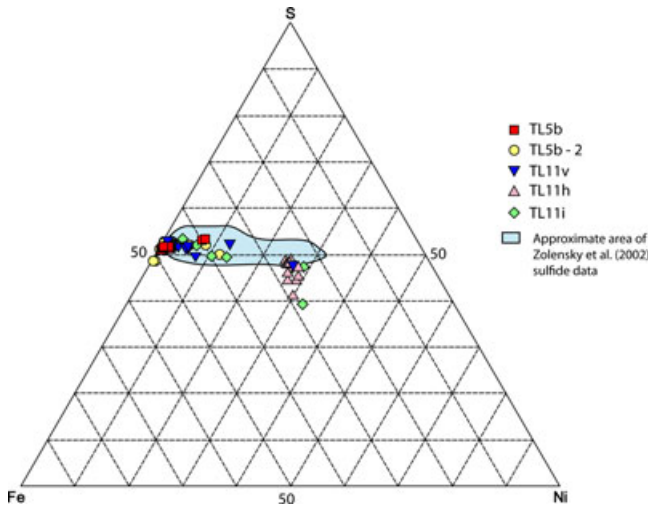

Fig. 2. Fe-Ni-S ternary diagram (atom%) showing range of sulfide compositions in the studied Tagish Lake samples. The light blue is the approximate range of compositions of sulfides studied by Zolensky et al. (2002).

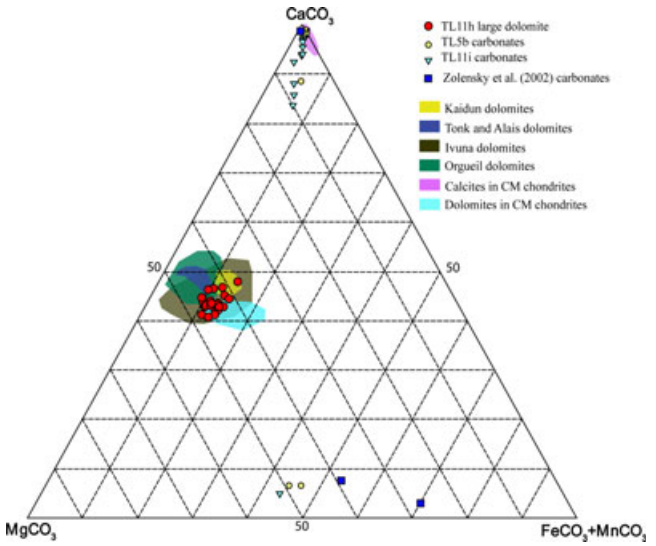

Fig. 3. Ternary diagram showing carbonate compositions (in mol%) with respect to $MgCO_3$-$CaCO_3$-$FeCO_3$+$MnCO_3$ from TL5b, TL11i, and TL11h along with three analyses of carbonates from Zolensky et al. (2002) and approximate fields of CI and CM dolomites (Endress and Bischoff 1996; Petitat et al. 2011).

morphologies have been observed in both CI and CR chondrites (e.g., Kerridge 1970; Weisberg et al. 1993).

Carbonates fall into three groups (formulae calculated based on two positive charges following Brandelik [2009] CALCMIN calculations). One group is Ca-rich containing small amounts of Fe and can be expressed as $[Ca_{0.97\text{-}0.98}Fe_{0.01\text{-}0.02}]CO_3$. Another group is also Ca-rich, but contains small amounts of both Fe and Mg, and small amounts of Si, Al, or Na and expressed as $[Ca_{0.75\text{-}0.97}Mg_{0.01\text{-}0.07}Fe_{0.01\text{-}0.05}Si_{0.01\text{-}0.03}Al_{0.01}Na_{0.01}]CO_3$. A third group is Mg- and Fe-rich with small amounts of Ca, Na, and Mn with a formula $[Mg_{0.45\text{-}0.47}Fe_{0.36\text{-}0.43}Ca_{0.04\text{-}0.06}Na_{0.02\text{-}0.03}Mn_{0.02\text{-}0.03}][C_{0.99\text{-}1.00}P_{0.00\text{-}0.01}]O_3$ (Fig. 3). Specimen TL5b contains all three compositional groups of carbonates. Three carbonates reported by Zolensky et al. (2002) have compositions similar to those we report here (Fig. 3). Zega et al. (2010) observed in their Tagish Lake sample a mixed-cation carbonate enriched in Fe and Mg with minor Ca and Mn, consistent with the third group of carbonates found in our studied samples. Carbonates of similar composition were found in CM2 chondrites (e.g., Benedix et al. 2003).

Most of the carbonates range from 3 to 10 μm in diameter, with rare grains reaching up to 30 μm. Only one large carbonate (100 × 200 μm) with an irregular, fine-grained rim (30–100 μm in thickness) that surrounds it was identified in specimen TL11h (Blinova et al. 2012). The composition of the rim is dominated by sheet silicates rich in Mg and Si with small random pockets of Mn-Ca carbonates. The average composition (Table 1) of this large carbonate grain is dominated by Mg and Ca, but with up to 2 wt% Mn. The chemical formula of the grain based on two charges is $[Mg_{0.38\text{-}0.47}Ca_{0.41\text{-}0.48}Fe_{0.09\text{-}0.12}Mn_{0.01\text{-}0.04}Na_{0.00\text{-}0.01}]CO_3$. The composition of each analysis (normalized to 100%) is plotted on a ternary CaO-MgO-(FeO+MnO) diagram (Fig. 3), along with the approximate compositional ranges of dolomites from CI and CM chondrites. The composition of the TL11h dolomite grain falls in the Ivuna field and slightly overlaps the fields of other CI and CM dolomites.

Composition of Other Minerals and Chondrule Mesostasis

Minerals such as phosphates and chromites are minor in Tagish Lake specimens. Phosphates were identified in all samples and most of them are fine-grained (<5 μm). Specimens TL11i and TL11h have the largest phosphate grains so far found in the studied specimens. One of them (in TL11h) is an irregular, large (approximately 500 × 250 μm), fluffy grain with low analytical totals (85 wt%), enriched in Ca and Mg (Table 1) and contains a cracked lithic fragment enriched in sheet silicates on one side of the grain. A phosphate grain in specimen TL11i is more compact (approximately 300 × 200 μm) and is situated outside of the main specimen mount as if plucked out during the mounting procedure, precluding determination of the textural and mineralogic context of this grain relative to the matrix. This grain also has low analytical totals (approximately 69 ± 7 wt%), possibly due to

porosity and/or some volatile component, and is enriched in Mg only (Table 1).

We found that the majority of the Tagish Lake type IIA chondrules in our samples contain spinel grains, consistent with the observations of Simon and Grossman (2003). These grains are enriched in Cr_2O_3 (42.6 ± 3.5 wt%) and Al_2O_3 (28.5 ± 3.9 wt%) (Table 1). Their compositions vary from 47% to 53% chromite (Chr = molar Cr/[2Ti+Cr+Al+Fe^{3+}]), 44% to 50% spinel (Sp = molar Al/[2Ti+Cr+Al+Fe^{3+}]), up to 0.02% magnetite (Mt = molar Fe^{3+}/[2Ti+Cr+Al+Fe^{3+}]), and up to 0.02% ulvöspinel (Usp = molar 2Ti/[2Ti+Cr+Al+Fe^{3+}]). One grain has the composition 36% Chr (=molar Cr/[2Ti+Cr+Al+Fe^{3+}]), 63% Sp (=molar Al/[2Ti+Cr+Al+Fe^{3+}]), and 0.02% Usp (=molar 2Ti/[2Ti+Cr+Al+Fe^{3+}]) more consistent with Mg-Al spinel.

We have also found an unknown phase in the altered lithic fragment in the TL11v-1 specimen. All lithic fragments are extremely fine-grained and much denser than the matrix surrounding them and contain forsterite and numerous sulfide grains, as well as unknown subrounded to rounded grains with low analytical totals (92–95 wt%). EDS identified these unknown grains as Mn-Ca silicate, enriched in MnO (24–25 wt%), CaO (28–30 wt%), and SiO_2 (34–35 wt%) with minor Al and Mg. The low analytical totals possibly point to a hydrous component (Table 1 in "Mesostasis and Other Phases"). The morphology of these unknown grains is similar to the grains found in the outer rim of the broken chondrule in TL5b (see below).

The mesostasis was surveyed in detail in two areas in the largest chondrule (Figs. 4a–d; and also see discussion below). Some areas of this chondrule contain microcrystallites (area "a" in Fig. 4c). The compositions of these areas have high analytical totals (99.99 wt%; Table 1 in "Mesostasis and Other Phases") and are comparable to the measurements of mesostasis in chondrules of type 2–3 meteorites reported by Brearley and Jones (1998) (Table 1). In other areas (e.g., area "b" on Fig. 4d), the mesostasis is hydrated, as indicated by low totals (approximately 76 wt%; Table 1 in "Other Phases"). The majority of chondrules in the studied samples contain similar hydrated mesostasis.

Composition of the Matrix and Fine-grained Rims around Chondrules

Matrix is defined as any fine-grained material that is interstitial to the obvious inclusions and chondrules (e.g., Browning et al. 1996). In the Tagish Lake specimens, this material is black and heterogeneous in macroscopic view. BSE imaging of matrix contains heterogeneous contrast due to numerous voids/pores, small (<2–3 μm) oxides, carbonates, and silicate grains. We used defocused (10 μm) and focused (2 μm) EPMA beam setups to determine the compositional variations in the matrix. In Table 2 (average of defocused and focused analyses), we present what we believe to be the analyses of the finest-grain fractions of the matrix. We acquired line scans on each sample with over 100 points for focused and over 50 points for defocused beam analyses. The majority of analyses have inconsistent results: some have low analytical totals (60–75 wt%), likely due to the presence of hydrous material and organics, or consistent with the highly porous nature of the measured samples; while others have higher analytical totals (90–93 wt%) possibly due to numerous small grains of oxides and silicates unevenly dispersed in the matrix, which are calculated as a part of the analyses. Therefore, we do not report average values based on totals from either line scans of focused and defocused beam analyses as it would not show the compositional variations of the sheet silicates found in the matrix of Tagish Lake, but rather a general composition of the matrix as a whole. We select only analyses that have totals similar to what is expected for the composition of sheet silicates (>80 wt%) and present averages of these analyses (see number of analyses in Table 2). A lithic fragment (dense, light colored in BSE, irregular sheet silicate–rich area) from specimen TL11i was also measured. From this sample, a higher number of analyses with totals of 82–87 wt% were obtained.

In Fig. 5, we plot both focused and defocused analyses of matrix composition on an Fe-Si-Mg (wt% element) diagram. Similar to Zolensky et al. (1993), the focused beam analyses (Fig. 5b) show more scatter relative to the defocused analyses, although the overall area coverage is the same. Based on these analyses, no pure smectite endmembers of sheet silicates are present in our samples. The majority of analyses fall between smectite and serpentine solid solutions, but some plot near the Fe-rich sheet silicates. Based on these results, the Tagish Lake matrix is dominated by a mixture of smectite and other sheet silicates. The analyses of each sample overlap with the other samples and appear to have similar variations in FeO. For example, TL5b analyses (Fig. 5a) spread across the whole coverage area. All samples show more variation in FeO (from a few wt% up to 60 wt%) than in MgO or SiO_2 (Table 2). The same variation can be seen in Tagish Lake data reported by Greshake et al. (2005) and Zolensky et al. (2002). One difference between our data and that of Zolensky et al. (2002) is in the S content as these authors disregarded the data with S > 1 wt% to avoid data points that were inconsistent with serpentine compositions (Zolensky et al. 2002). In our experience,

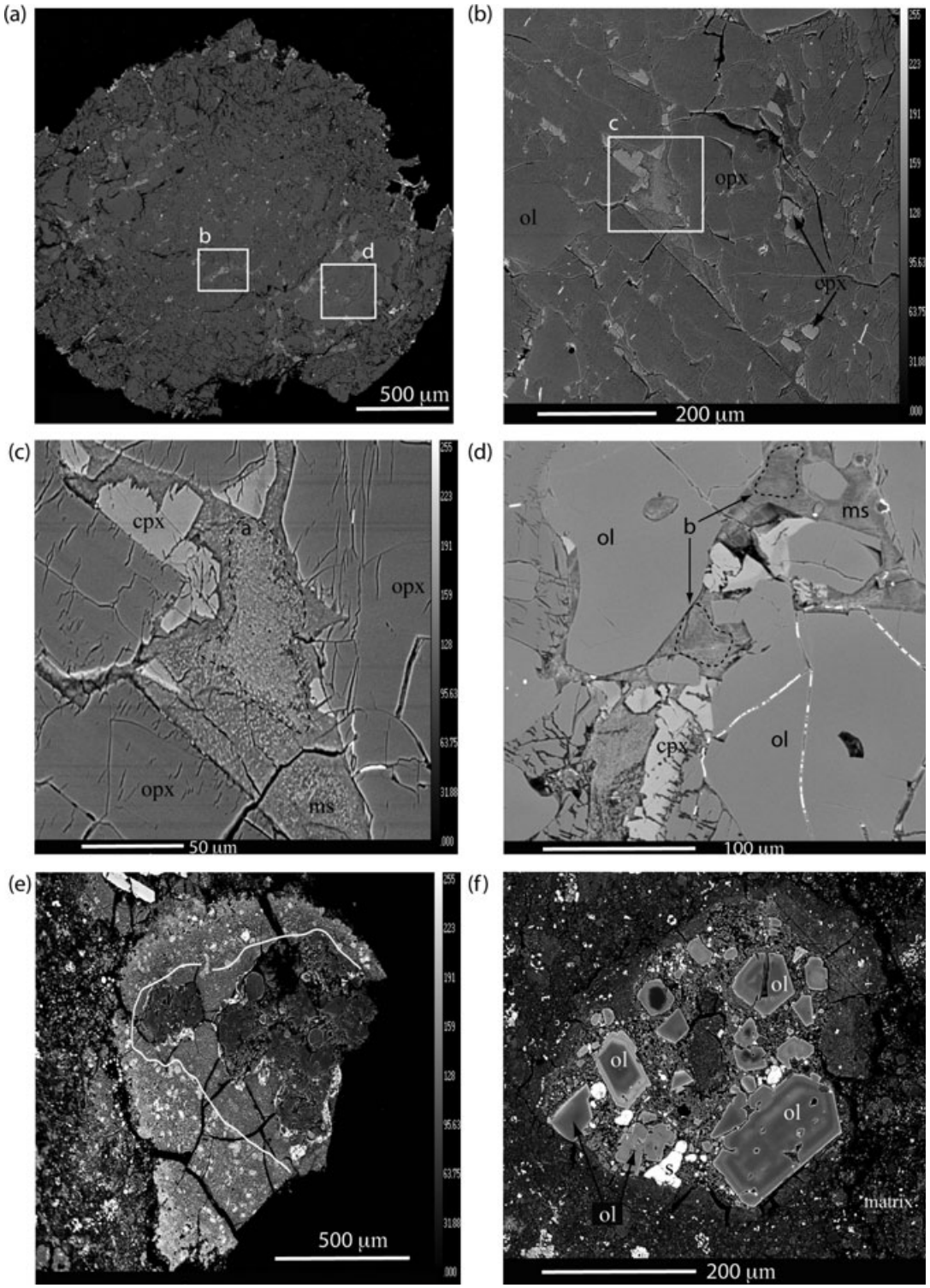

Fig. 4. Backscattered electron images of: a) A large chondrule from TL5b, approximately 2 cm in diameter; b, c, d) Enlargement of a partially crystallized mesostasis (see text for details). In (c), the light gray mineral is clinopyroxene and dark gray is orthopyroxene. e) A broken chondrule with a thick rim from TL5b. The rim consists of two parts divided by the white line (see text for details). f) Chondrule from TL11i with normally and oscillatory-zoned olivines. The largest olivine has a euhedral shape and exhibits oscillatory zoning ($Fo_{70\text{-}79}$). Other olivine grains within it have normal zoning from Mg-rich cores ($Fo_{79\text{-}99}$) to Fe-rich rims ($Fo_{61\text{-}74}$).

Table 2. Average matrix composition.

Sample	N	SiO_2	Al_2O_3	Cr_2O_3	FeO	MnO	MgO	CaO	Na_2O	K_2O	NiO	TiO_2	V_2O_3	Cl	S	Total
(1)		34.02	11.97	0.33	16.61	0.38	22.96	0.65	0.18	0.05	0.05	0.10	na	na	0.06	87.43
(2)		42.33	1.07	0.71	10.72	0.15	32.18	0.09	0.05	0.02	0.05	0.08	na	na	0.06	87.57
(3)		30.62	13.66	0.31	27.14	0.35	15.73	0.60	0.39	0.06	0.05	0.09	na	na	0.06	89.06
(4)		39.35	3.56	0.56	14.34	0.20	28.26	0.14	0.13	0.05	0.15	0.09	na	na	0.05	86.96
(5)		26.42	19.24	0.08	20.47	0.23	16.97	0.10	0.26	0.11	0.03	0.09	na	na	0.11	85.45
G[a]		22.40	1.90	0.32	16.30	0.20	15.20	0.97	0.22	0.06	1.50	na	na	na	3.90	63.00
10 μm (defocused) beam																
TL5b	13	24.77	3.01	0.37	28.50	0.23	17.78	0.91	0.34	0.16	1.82	0.11	0.01	0.29	5.74	84.01
stdev		6.36	0.81	0.15	12.79	0.11	6.91	0.94	0.13	0.06	1.50	0.04	0.01	0.08	2.23	3.98
TL11i LF[#]	18	32.18	2.44	0.60	22.11	0.19	18.73	0.51	0.50	0.18	2.15	0.22	0.01	0.06	6.76	86.62
stdev		2.09	0.18	0.17	4.16	0.06	1.26	0.16	0.05	0.03	0.73	0.04	0.01	0.01	2.09	1.89
TL11i	5	27.44	2.05	0.32	28.27	0.10	16.75	0.26	0.47	0.15	1.19	0.09	0.01	0.23	5.60	82.90
stdev		4.93	0.33	0.06	8.63	0.02	1.55	0.13	0.10	0.07	0.71	0.03	0.01	0.06	2.80	2.61
TL11v-1	32	29.28	2.30	0.38	23.23	0.26	19.02	1.37	0.73	0.05	1.66	0.12	0.01	0.06	6.22	84.69
stdev		2.55	0.42	0.07	3.62	0.07	3.73	1.59	0.15	0.01	0.39	0.05	0.01	0.04	1.63	3.08
TL11v-2	6	24.54	1.84	0.42	29.69	0.12	14.85	0.34	0.83	0.11	1.28	0.12	0.01	0.26	5.93	80.32
stdev		9.30	0.63	0.25	12.65	0.05	2.73	0.12	0.13	0.04	0.47	0.03	0.01	0.05	2.24	4.40
TL11h	4	31.15	2.48	0.38	20.78	0.11	20.48	0.44	0.52	0.10	0.91	0.14	0.01	0.35	3.85	81.67
stdev		6.11	0.51	0.07	8.79	0.07	3.88	0.17	0.14	0.03	0.42	0.06	0.00	0.10	2.45	1.86
2 μm (focused) beam																
TL11i LF[#]	28	34.92	2.65	0.49	18.13	0.15	21.16	0.44	0.40	0.18	1.26	0.20	0.01	0.05	5.07	85.07
stdev		3.96	0.41	0.24	5.13	0.07	3.21	0.22	0.13	0.04	0.71	0.05	0.01	0.01	2.69	2.52
TL11i	31	26.37	1.99	0.32	27.48	0.12	16.34	0.48	0.39	0.17	1.38	0.13	0.01	0.19	7.61	82.96
stdev		6.16	0.45	0.10	12.55	0.07	3.98	0.55	0.16	0.10	1.03	0.06	0.01	0.10	4.65	3.16
TL11h	19	30.16	2.15	0.44	23.03	0.17	21.44	0.33	0.44	0.08	0.94	0.10	0.01	0.25	4.31	83.81
stdev		7.55	0.80	0.40	12.94	0.19	9.57	0.22	0.21	0.05	0.84	0.07	0.01	0.08	3.44	3.08
TL11v-1	31	30.38	2.69	0.43	23.03	0.30	19.56	0.83	0.72	0.06	1.69	0.12	0.01	0.06	6.13	86.00
stdev		5.77	2.01	0.23	6.62	0.15	4.90	1.04	0.20	0.02	0.61	0.03	0.01	0.03	1.89	3.65
TL11v-2	4	35.55	2.65	0.65	14.47	0.06	20.38	0.28	0.64	0.11	1.05	0.10	0.02	0.22	3.77	79.93
stdev		5.26	0.38	0.25	3.04	0.03	4.21	0.07	0.22	0.00	0.61	0.02	0.01	0.11	2.48	3.91

TL11v-1 and TL11v-2 are two chips of the disaggregated TL11v sample (see text for discussion).
(1)–(5) analyses from Zolensky et al. (2002), Table 3.
[a]Average matrix data from Greshake et al. (2005).
na = not available; LF = lithic fragment from sample TL 11i.

by excluding analyses with S > 1 wt% more than 95% of the data we collected is eliminated.

Tomeoka and Buseck (1988) attributed large variations in Fe content in Orgueil matrix to the presence of ferrihydrite. Greshake et al. (2005) explained the variations of Fe-rich compositions by invoking the heterogeneous distribution of magnetite, sulfides, and rare Fe-rich sheet silicates. As we have not observed any ferrihydrite in our sample through either EPMA or TEM, we conclude that the variations in FeO are attributable mainly to the presence of magnetite and Fe-rich sheet silicates. The mineralogy of the lithic fragment matrix, based on our TEM measurements (see below), was determined as a mixture of saponite and serpentine. This is consistent with the compositional range of this material measured by EPMA, which extends from the middle of the smectite-serpentine region up to and just above the serpentine solid solution line (green diamonds in Fig. 5). The analyses of the matrix in our Tagish Lake specimens cover a similar field as CM chondrites (Zolensky et al. 1993) and overlap the Ivuna field (Tomeoka and Buseck 1988) (Fig. 5).

Chondrules are the only objects in the Tagish Lake samples that have fine-grained rims (FGRs) (e.g., Zolensky et al. 1993) similar to the ones described previously in this meteorite (e.g., Greshake et al. 2005; Izawa et al. 2010; Takayama and Tomeoka 2012). The boundary between the rims and matrix is gradational, whereas that with the chondrule's surface is sharp. The overall composition of the FGRs is comparable to the Tagish Lake matrix except that they contain a lower abundance of Ca carbonates and higher concentrations of S. Similar observations were noted by Greshake et al. (2005) and Takayama and Tomeoka (2012). Rims are extremely fine-grained (<0.2 μm) and contain sulfides (Fe-Ni) and rare low-Ca pyroxene and forsterite. Some

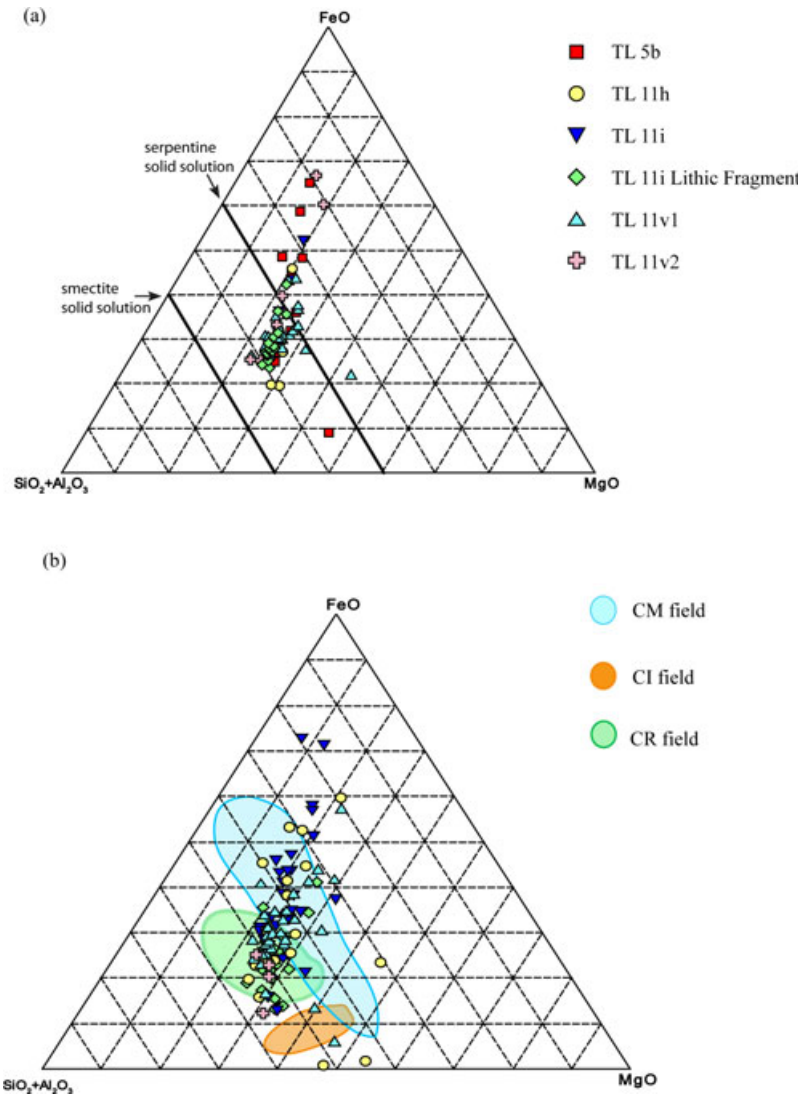

Fig. 5. Si-Mg-Fe ternary diagrams (wt%) showing compositional variations of matrix from the Tagish Lake samples: a) defocused (10 μm) beam; b) focused (2 μm) beam. CM, CR, and CI fields are from Zolensky et al. (1993) and Weisberg and Huber (2007).

rims completely surround the chondrule, while others appear to be broken. In addition, the rims have numerous fractures that do not extend into the matrix. One large chondrule in TL5b has a rim of varied thickness (from 10 to 200 μm) and two different compositions (Fig. 4e). The outer part of the rim is enriched in Fe and S with prominent subrounded-to-rounded grains (possible carbonates), and the inner part is devoid of these grains and depleted in both Fe and S (Fig. 4e). The transition between the two parts of the rim is abrupt. The majority of chondrule rims were found to have similar compositional and textural characteristics although thickness varies. Similar Fe-S gradational FGRs have been described in CM and CR chondrites (e.g., Metzler et al. 1992; Hanowski and Brearley 2000, 2001; Zega et al. 2003; Chizmadia and Brearley 2008; Abreu and Brearley 2010).

EPMA Observations: Component Abundances and Textures in Tagish Lake Specimens

We used BSE images (Figs. 6a–e) to observe and establish the quantitative abundance of components such as chondrules, matrix, lithic fragments, isolated silicates, sulfides, carbonates, and magnetites to determine the mineralogic differences among the samples. We used these differences as a foundation for determining the alteration degree in each sample. We consider chondrules

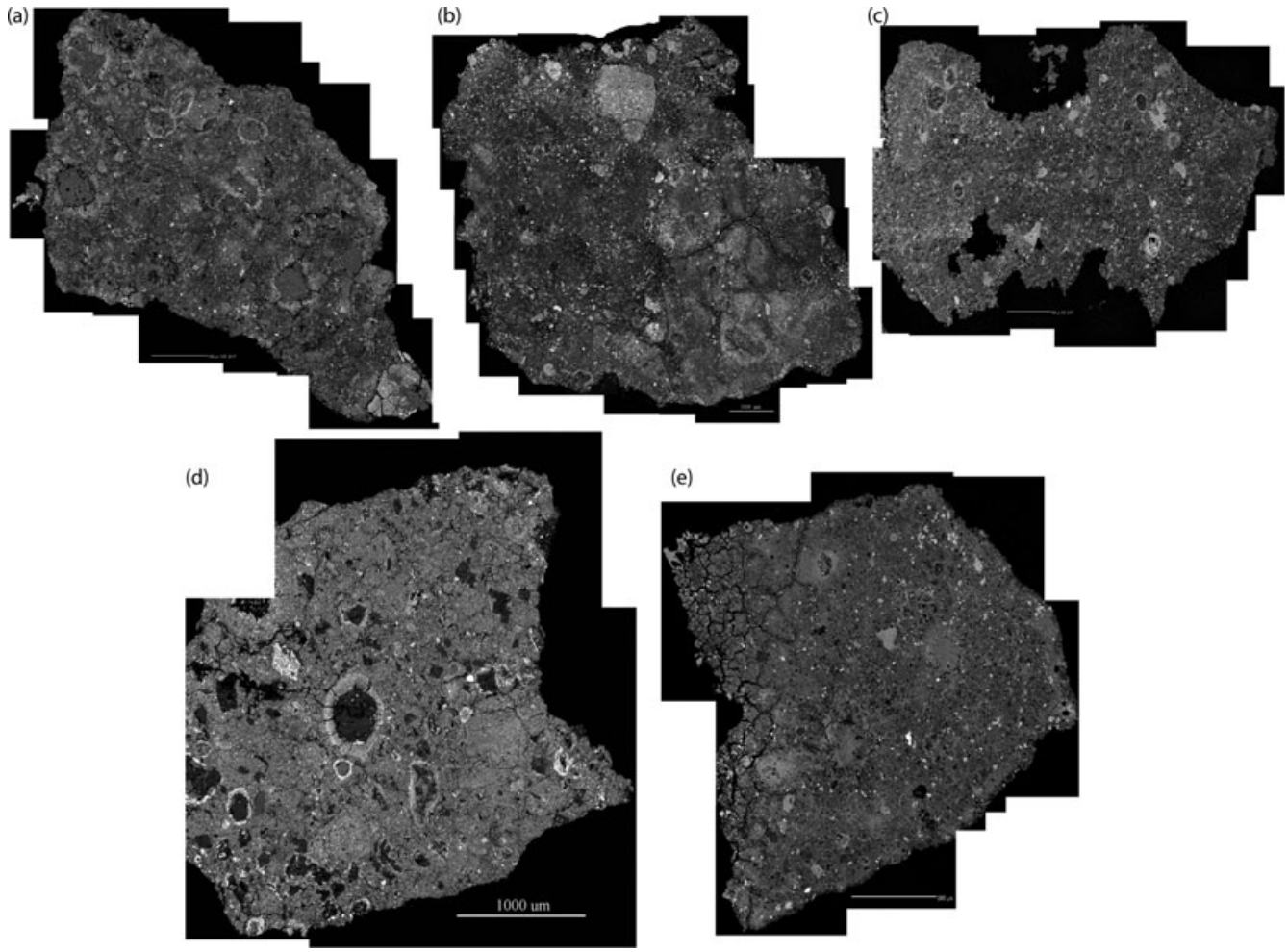

Fig. 6. Backscattered electron images of the studied Tagish Lake samples: a) TL5b; b) TL11h; c) TL11i; d) TL11v-1; and e) TL11v-2. The last two images are of two chips from TL11v.

and isolated silicates, such as olivine and pyroxene grains, as primary components most likely of nebular origin (Brearley and Jones 1998). We used BSE images to calculate the modal abundance of these components and fine-grained lithic fragments, which are composed of sheet silicates mixed with fine-grained magnetite and sulfide. The abundances of sulfides, carbonates, and magnetites, which are products of alteration and, hence, are secondary components, were visually estimated by comparing BSE images of samples. Matrix abundance was calculated as the difference between 100% and the rest of the components.

We define chondrules as all objects that preserve rounded-to-semirounded exterior surfaces either partially altered or completely pseudomorphed, and that look like chondrules as described by Brearley and Jones (1998). Because mesostasis in the studied samples is mostly replaced by hydrous phases (Table 1), except for the large TL5b chondrule (see below), the main key parameter that is used to distinguish different degrees of alteration in the Tagish Lake chondrules is the presence of olivine and pyroxene grains inside these objects that are visibly intact, nonhydrated, and unaltered to sheet silicates. We consider a chondrule as slightly altered when the interior silicate grains show no evidence of replacement by secondary minerals (e.g., Fig. 4). A chondrule is considered to be highly altered when the interior is completely replaced by sheet silicates (e.g., Figs. 7a–d) including all primary olivine and pyroxene phenocrysts. We have observed "pseudomorphs of opaque nodules" in the majority of chondrules, similar to those described by Takayama and Tomeoka (2012). Our observations indicate that their abundance has a positive correlation with the degree of chondrule alteration.

Specimen TL5b (Fig. 6a) contains the highest number of chondrules (approximately 30 vol%). The olivine grains in these chondrules show no evidence of alteration. Pyroxene grains, on the other hand, are

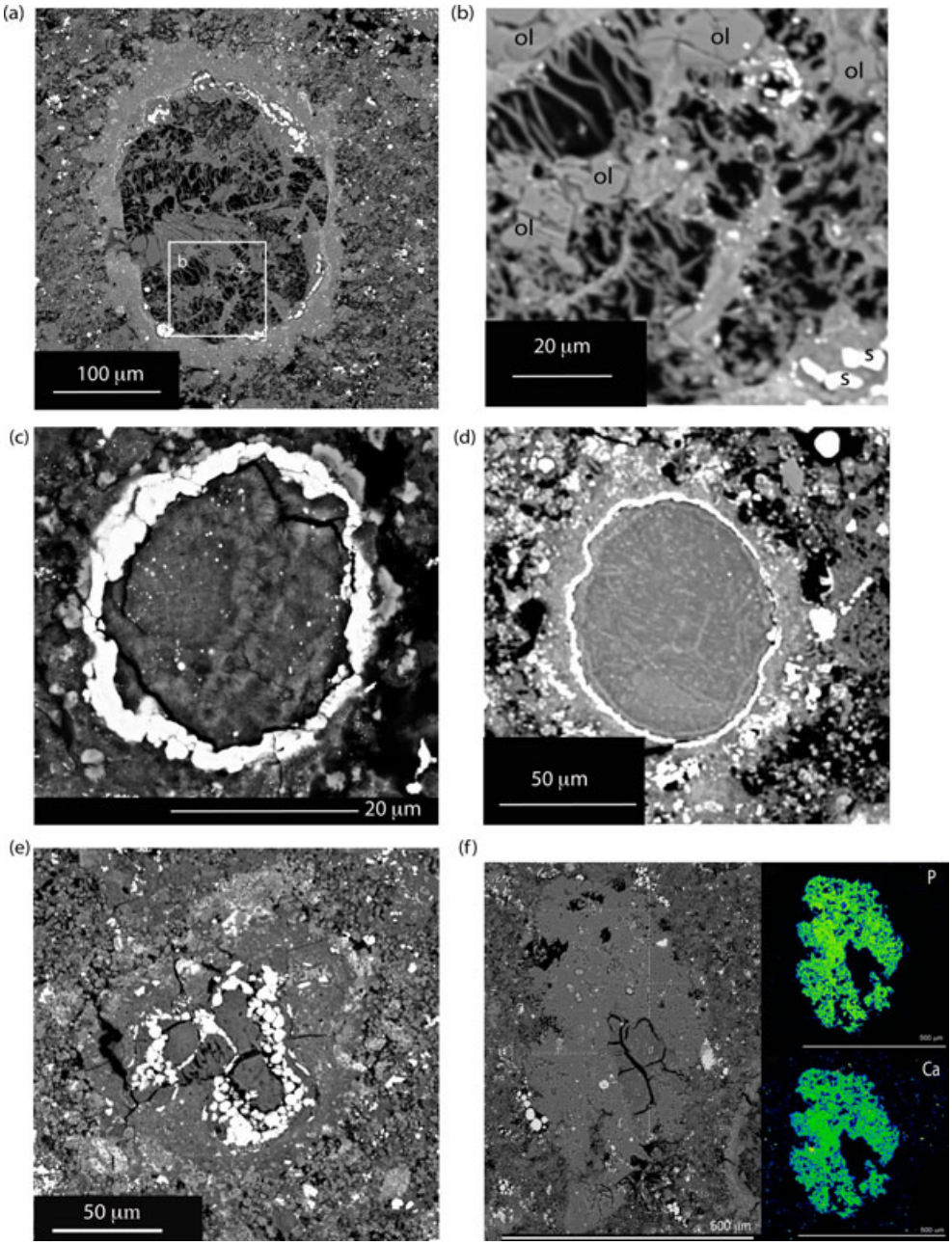

Fig. 7. Backscattered electron images of (a) chondrule from TL11h with extensively altered silicate grains replaced by sheet silicates. b) A close-up of (a) to show the morphology of the sheet silicates that are growing as distinctive arrays into the voids (black areas); ol = olivine; s = sulfides; c) an altered chondrule from TL11h with a sulfide/magnetite rim and "flower-like" morphology produced by sheet silicates, and (d) an altered chondrule from TL11h with a fine-grained, dense texture. e) pseudomorphed chondrule from TL11i containing remnant olivine grains (center) altered by sheet silicates and surrounded by magnetite/sulfide grains. d) Ca-P aggregate (BSE map [left image], Ca [lower right], and P [upper right] elemental maps of the same BSE map) found in TL11h only. It has a cracked lithic fragment in the lower right corner of the aggregate.

altered to various degrees, similar to the observations of Takayama and Tomeoka (2012) in other samples of the Tagish Lake meteorite. Therefore, we consider the chondrules in TL5b as slightly altered compared with chondrules in other studied samples. All observed chondrules in this sample are porphyritic Type I (Fe-poor; McSween 1977) with hydrated mesostasis. The TL5b specimen is also distinguished from the other samples by the size of chondrules, which vary from a few microns to a few millimeters in diameter. Most

chondrules in TL5b are small (up to 500 μm) and have a deformed shape: either hourglass or ellipsoidal. During processing of specimen TL5b, a large (approximately 2000 μm in diameter) chondrule fell out of the porous matrix (Fig. 4a). This chondrule is nearly perfectly spherical and is only moderately altered on its exterior. It is a porphyritic type I chondrule dominated by two types of pyroxene ($En_{96}Fs_{3.6}Wo_{0.4}$ and $En_{62.3}Fs_{4.2}Wo_{32.5}$) and olivine ($Fo_{95\text{-}96}$) with Mn enrichment in olivine rims (MnO up to 1 wt%). This chondrule is also distinguished from other chondrules in that some areas of mesostasis have high analytical totals (Table 1; Fig. 4). This suggests a glass with microcrystallites, either from quench or from the beginnings of devitrification. We believe that those high totals rule out significant hydration of this specific chondrule (Table 1).

Fine-grained matrix (approximately 18–20 vol%) in TL5b, consisting of a mixture of smectite and serpentine, occurs interstitially between the anhydrous components. In addition to the highest number of chondrules, specimen TL5b also contains the lowest proportion of lithic fragments (approximately 2 vol%) and the most abundant isolated unaltered silicate grains. These grains are dominated by forsterite ($Fo_{95\text{-}99}$) (up to 5–8 vol%) with minor pyroxene (approximately 2–3 vol%). Some of these Fo_{99} grains are large (400 × 500 μm) with thin fractured rims and rare sulfide inclusions. The specimen contains framboids of magnetites after sulfide crystals similar to the ones reported by Zolensky et al. (2002). Other sulfides (Fig. 8) can be found as solitary grains or in clusters (<10 μm) with nonexsolved and exsolved morphologies. The exsolved morphologies in all studied samples are: (1) pentlandite inside pyrrhotite grains with characteristic "flame" textures, (2) partially coarsened, en echelon blades of pentlandite in pyrrhotite, and (3) massive pentlandite intergrowths with pyrrhotite (Fig. 8). We have not observed any sulfide veins in either TL5b or other samples as was reported by Bullock et al. (2005) in a CM1 clast in Tagish Lake.

Specimen TL11i (Fig. 6b) shows more extensive evidence of alteration than TL5b. It is dominated by fine-grained matrix (up to 50 vol%). The majority of chondrules (approximately 5 vol%) are pseudomorphed, containing mostly sheet silicates and are mostly devoid of any unaltered silicate grains (Fig. 7e). This sample, however, contains one porphyritic type IIA chondrule with unaltered zoned olivines, remnants of pyroxene grains altered to sheet silicates, some sulfides, and a hydrated mesostasis (Fig. 4f). Carbonates (approximately 4 vol%) occur in lower abundance, but larger size than in TL5b reaching up to 30 μm. Clusters of fine-grained (<20 μm in diameter) framboidal and plaquette magnetites (approximately 15 vol%) and isolated olivine grains (up to 5 vol%) are dispersed throughout the matrix. Some magnetite framboids and plaquettes are found in clusters with sulfides. Sulfides show similar morphologies (Fig. 8) to TL5b. The abundance of sulfides is similar to carbonates.

Specimen TL11h (Fig. 6c) has characteristics intermediate to TL5b and TL11i. The abundance of chondrules appears to be closer to TL5b (approximately 25 vol%), but they are smaller in size (50–200 μm) and have more diverse morphologies than TL5b. The inside of one chondrule (Fig. 7a) surrounded by a FGR appears to be extensively altered: silicate grains are partially replaced by sheet silicates, with the latter growing into numerous voids as distinctive arrays (Fig. 7b). We also observe altered chondrules that have sulfide/magnetite rims of various thicknesses (approximately 2–5 μm) with diverse interior textures: one (Fig. 7c) is similar to the coronal, "flower-like," morphology described below in the focused-ion-beam (FIB) section of TL11i-2, whereas another chondrule is fine-grained, dense, and completely altered to sheet silicates with a sulfide rim around it (Fig. 7d). Greshake et al. (2005) found similar rims, although with larger thicknesses (up to 35 μm) and composed entirely of sulfides. On the basis of these morphologies, we infer that TL11h chondrules are more altered than TL5b, but less altered than TL11i. The abundance of irregular lithic fragments (up to 10 vol%) in TL11h is similar to TL11i, but they are much smaller (largest is approximately 100 μm); some contain cracks and are more fragmented. One of the lithic fragments is embedded in the lower right corner of the Ca-Mg phosphate grain (Fig. 7f). Fine-grained magnetites occur as isolated grains, in framboidal and plaquette clusters, or as pseudomorphs after sulfides (15 vol%). Most carbonates are fine-grained, with the exception of one large (100 × 200 μm) Mn-rich carbonate grain (MnO up to 3.5 wt%), and evenly distributed throughout the sample. Carbonate modal abundance is close to that of TL5b (up to 11 vol%). Sulfides are rare (1–2 vol%), but their microstructures are similar to TL5b and TL11i. Fine-grained matrix, rich in sheet silicates, is similar in abundance to TL11i (up to 40 vol%).

Specimen TL11v is a mixture of fragments as it was collected as a disaggregated sample. The two chips picked for this study (Figs. 6d and 6e) have different abundances of components. Chip one (TL11v-1; Fig. 6d) is similar in all respects to TL5b. This chip contains higher abundances (up to 10 vol%) of large (100–150 μm) isolated silicate grains (the majority are forsteritic olivines) and chondrules (up to 40 vol%). The majority of these chondrules have intact olivine and

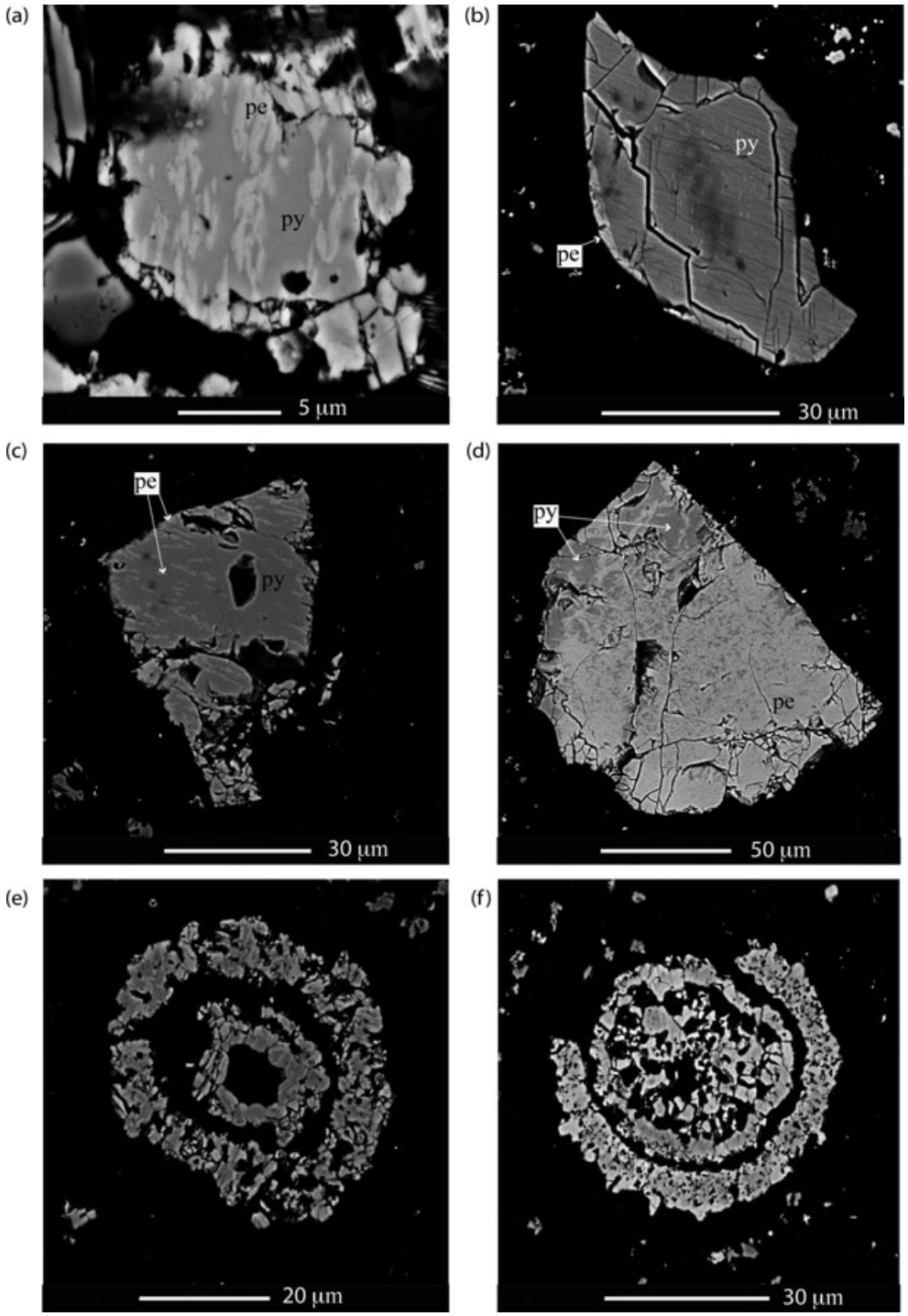

Fig. 8. Backscattered electron images of individual sulfide grains showing the variety of morphologies found in the Tagish Lake samples: a–d) exsolved pentlandite (light gray, "pe") in pyrrhotite (dark gray, "py"); e–f) "bull's-eye" morphology exhibiting distinctive core and shell separated by a gap.

rare pyroxene grains with some sulfides and are therefore less altered compared with chondrules in the second chip. The abundance of components in the second chip (TL11v-2; Fig. 6e) is similar to TL11h, although magnetite differs in size. Large (up to 30 μm) framboidal magnetites are found in clusters (approximately 17 vol%) along with sulfides (approximately 15 vol%). Chondrules have been

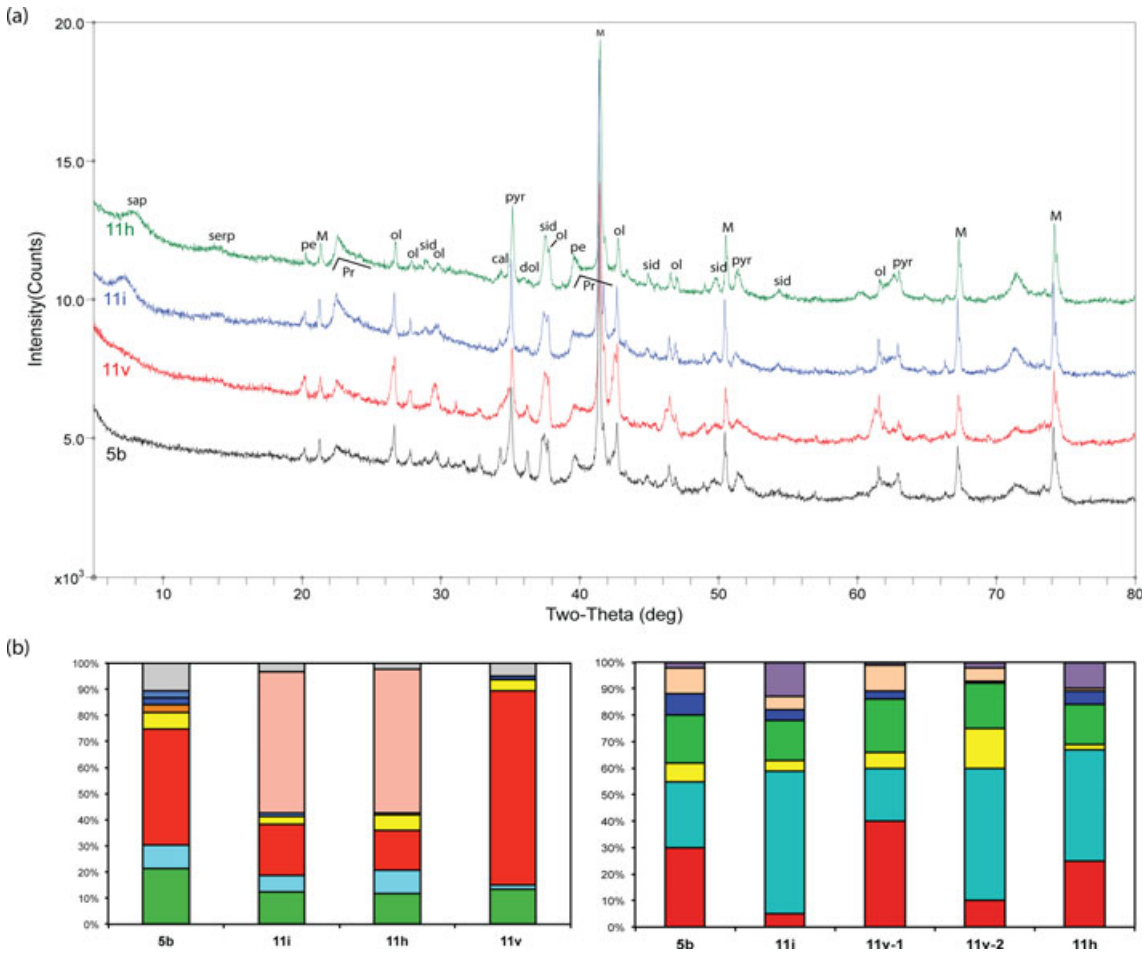

Fig. 9. a) Interpreted XRD diffractograms for powdered TL5b, TL11h, TL11i, and TL11v samples. Peaks are as follows: sap, saponite; serp, serpentine; pe, pentlandite; M, magnetite; ol, olivine; sid, siderite; cal, calcite; dol, dolomite; pyr, pyrrhotite; pr, prism reflection of saponite. b-left) Graphical representation of modal differences in samples calculated by Rietveld refinement method. Colors: gray—amorphous material; light pink—clinochlore; light blue—calcite; dark blue—dolomite; orange—enstatite; yellow—pyrrhotite; red—forsterite; turquoise—siderite; green—magnetite. b-right) Graphical representation of modal differences in samples manually observed using EPMA. Colors: purple—lithic fragments; light pink—isolated silicates; dark blue—carbonates; green—magnetite; yellow—sulfides; turquoise—matrix; red—chondrules.

strongly altered to sheet silicates and comprise ≤10 vol% of the section. The isolated forsterite grains reach up to 100 μm in size and comprise approximately 5 vol% of the sample. All components are embedded in fine-grained matrix (approximately 50 vol%). Carbonates are rare (1–2 vol%). This chip also has a part of a fusion crust that takes up 20% of the chip.

In summary, we make two major observations from the EPMA results: (a) the samples differ from each other in abundances of both primary (nebular) components such as chondrules and isolated silicates, and secondary (alteration products) such as magnetites, carbonates, and sheet silicates; and (b) the primary components have been altered to varied degrees in each sample. TL5b has the highest number of mildly altered chondrules compared with those in other samples. It also contains a large chondrule with devitrified mesostasis, which rules out substantial alteration of TL5b. Sample TL11i, on the other hand, contains the smallest volume percent of pseudomorphed chondrules. This sample, however, contains the highest volume percent of lithic fragments and sheet silicate-dominated matrix compared with other studied samples.

To substantiate the EPMA component estimations and the above conclusion, we used XRD to determine the abundance of minerals. This method determined that components such as forsterite, magnetite, pyrrhotite, enstatite, dolomite, calcite, clinochlore (representative of sheet silicates), and an amorphous phase occur in varied abundances (Fig. 9; Table 3). The refinement suggests that siderite also occurs in the

Table 3. Bulk rock mineralogy of Tagish Lake samples: comparison by EPMA, XRD, and literature data.

		XRD									EPMA						(a)		(b) HG-42		HG-11		MM-38	
	Density (g/cm^3)[a]	5b wt %[c]	5b vol %[d]	11i wt %[c]	11i vol %[d]	11h wt %[c]	11h vol %[d]	11v wt %[c]	11v vol %[d]		5b vol %[e]	11i vol %[e]	11h vol %[e]	11v-1 vol %[e]	11v-2 vol %[e]		wt %	vol %	wt %	vol %	wt %	vol %	wt %	vol %
Forsterite	3.28	39	44	19	20	15	15	68	74	Chondrules	30	5	25	40	10	Olivine (Fo_{100})	8	7	4	3	9	7	8	7
Magnetite	5.18	30	21	19	12	18	12	19	13	Magnetites	18	15	15	20	17	Magnetite	8	5	13	7	9	5	12	6
Pyrrhotite	4.60	8	6	4	3	8	6	6	4	Sulfides	7	4	2	6	15	Pyrrhotite	9	5	10	6	16	11	10	6
Enstatite	3.20	3	3	n/d	n/d	n/d	n/d	n/d	n/d	Isolated silicates	10	5	1	10	5	Pentlandite	1	0	≤3	≤3	≤3	≤3	≤3	≤3
Dolomite	2.84	2	3	n/d	n/d	n/d	n/d	1	1	Carbonates	8	4	5	3	1	Fe-Mg carbonate	14	12	13	7	4	3	5	3
Siderite	3.96	10	9	7	6	10	9	2	2	Lithic fragments	2	13	10	1	2	Calcite			≤3	≤3	5	6	≤3	≤3
Calcite	2.71	2	2	1	1	0	1	n/d	n/d	Matrix	25	54	42	20	50	Saponite-serpetine	60	71	57	69	55	68	55	68
Clinochlore (the best fitted)	3.00	n/d	n/d	48	54	48	55	n/d	n/d							Gypsum			8	9	≤3	≤3	10	11
Amorphous[b]	2.65	7.6	10.7	2.6	3.4	1.7	2.2	3.6	4.9							Talc			≤3	≤3	n/d	n/d	n/d	n/d
Total		100	100	100	100	100	100	100	100								100	100	105	101	98	100	100	101

[a]Source: www.mindat.org.
[b]Amorphous density = silica density.
[c]Determined wt% of each phase by Rietveld refinement method (XRD).
[d]Calculated volume percent based on wt% from XRD.
[e]Estimated volume percent by EPMA observations.
n/d = not detected or determined by the method.
Sources: (a) Bland et al. (2004); (b) Izawa et al. (2010) selected samples.

specimens, but we have not analyzed any grains with this composition. Siderite, however, was reported by Zolensky et al. (2002). All samples were found to contain abundant clay minerals and an amorphous phase, but further identification was not possible because appropriate reference spectra/models for the Rietveld refinement are not available in the WPF module of JADE 9.0 software that we used. The results from this exercise showed that specimen TL11h and TL11i are very similar, especially in the content of clay-like material (up to 55 vol%), while the bulk of specimen TL5b has a higher peak for an amorphous phase. The mixed specimen TL11v has up to 74 vol% of forsterite component, while specimen TL5b has the highest content of magnetite (up to 21 vol%) in bulk XRD. Carbonate abundance varies dramatically in each specimen. According to XRD, siderite appears to be present in all samples, whereas only calcite and dolomite occur in TL5b.

Results from EPMA-based abundance estimates (Fig. 9c) and those obtained by Rietveld analysis (Fig. 9b) are comparable within the error (10%). In both methods, specimens TL11h and TL11i show a high percentage of sheet silicates (clinochlore in XRD and matrix in EPMA data). For specimen TL5b, we identified up to 30 vol% of chondrule-like objects through EPMA observation. This observation is consistent, within error (10%), of the Rietveld calculations, which show up to 40% of "forsterite" component, which could be represented as either chondrules or isolated silicates. Specimen TL11v is a mixture of various fragments (described above), and so it is not surprising that our EPMA observations are not reflected in XRD data.

The majority of the data from both methods support each other; however, there are some differences in sheet silicate, magnetite, carbonate, and sulfide abundances. This could be related to the fact that Rietveld refinement is a semiquantitative method that employs the least-squares analysis, which in turn is appropriate only if (a) the data points have an associated Gaussian error distribution and (b) the proposed calculated model (i.e., an ideal crystal) taken from a database is a complete representation of the observed data (David 2004). Even though the first condition is usually satisfied, such heterogeneous planetary materials as Tagish Lake will inevitably have uncertainties with the second condition as no database will fit and/or fully cover its mineralogic heterogeneity (e.g., Howard et al. 2009, 2011). Other sources of errors such as preferred orientation, surface roughness, assumption of infinite samples thickness, etc., could also contribute to observed differences (e.g., David 2004; Izawa et al. 2010).

TEM OBSERVATIONS OF THE MATRIX

We used TEM to gain further insights into mineralogic and textural variations among the specimens. We investigated whether the macroscopic variations are mirrored at the submicron level in the matrix of each sample. Blinova et al. (2011) reported the preliminary TEM results on the Tagish Lake matrix.

Specimen TL5b Matrix

The TL5b FIB section contains large areas of amorphous groundmass and pores held together by epoxy (Figs. 10a and 10b). Porosity in Tagish Lake is high and thought to be primary (Brown et al. 2002). Rare areas of the groundmass contain poorly ordered, fine-grained silicates with ribbon-like structures mixed in with abundant amorphous material. The boundary between the two is usually gradational. Qualitative EDS analyses of the amorphous material show that it is rich in Si, Fe, Al, Ni, and S. Subhedral and anhedral sulfides (1–3 μm wide) occur in isolated domains. These domains contain nanosulfides of various shapes and sizes, e.g., spheres and rods (approximately 100–200 nm wide, respectively). The section contains a large grain (3 × 4 μm) with EDS-determined composition and *d*-spacings measured via SAED consistent with calcite. The carbonate grain is irregular in shape and consists of several subgrains.

Specimen TL11i Matrix

We made two FIB sections of specimen TL11i: 11i-1 and -2 (Fig. 11). Section 11i-1 was extracted from the part of the matrix that appears dark and porous on the macroscopic scale in SEM-BSE images, representative of typical matrix in TL11i and other samples (Figs. 11a and 11b). On the TEM scale, this section contains heterogeneously distributed sulfides (bands and patches), most of which have subhedral morphologies (up to 1.2 μm), but minor rods (up to 0.5 μm) also occur. Sheet silicates, exhibiting sinuous textures, occur interstitial to the sulfides, are enriched in Mg and have varied degrees of order. Measurements of HRTEM images of ordered regions reveal lattice-fringe spacings of 0.10–0.11 nm, consistent with saponite, and up to 0.14 nm, suggesting a chlorite-type phase (Fig. 12), similar to observations made by Zolensky et al. (2002). The FIB section of 11i-1 also contains two large calcite grains (≤3 × 1.5 μm) and several euhedral rod-shaped olivine grains, both identified by EDX. Overall, this matrix section is highly porous with large (1–2 × 3–4 μm), irregular cavities filled with epoxy and devoid of any minerals. Its porosity is similar to FIB section TL5b.

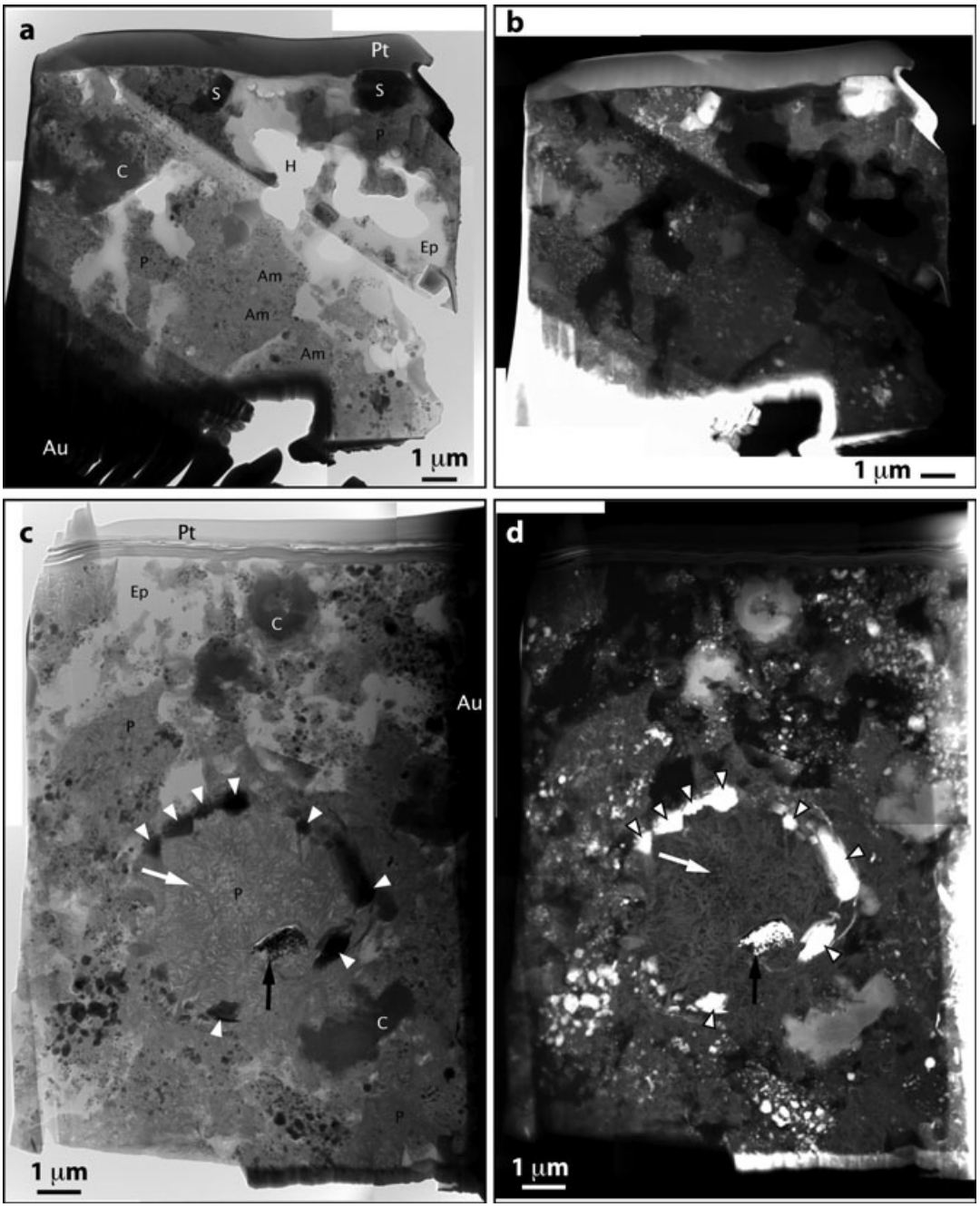

Fig. 10. Bright-field and HAADF-STEM images showing the FIB sections of TL5b (a, b) and TL11h (c, d). The middle part of the TL11H FIB section (c, d) contains a pseudocore-shell structure in which the core (white arrow) is composed of ribbon-like sheet silicates and a sulfide shell (arrowheads) that is discontinuous around the core. A phosphate-rich grain (black arrow) occurs near to the bottom-right of the structure and is partially embayed by sheet silicates on its lower edge. Pt = platinum; Au = gold; H = hole; Ep = epoxy; S = sulfides; C = carbonates; P = phyllosilicates; Am = amorphous material.

Section 11i-2 was extracted from a lithic fragment (Figs. 11c and 11d). The top part of FIB section of 11i-2 contains a compact area composed entirely of sheet silicates with a coronal, "flower"-like, microstructure (Fig. 13). This morphology has a compact core (diameters range approximately 0.3–1 μm) composed of sulfides/oxides and fine-grained sheet silicates curled onto each other from which bundles of sheet silicates (0.05 × 0.4 μm) radiate. In some areas, sheet silicates in the core and those radiating from it have a 0.7 nm basal spacing, consistent with the serpentine structure. In comparison, other parts of the coronal, "flower"-like,

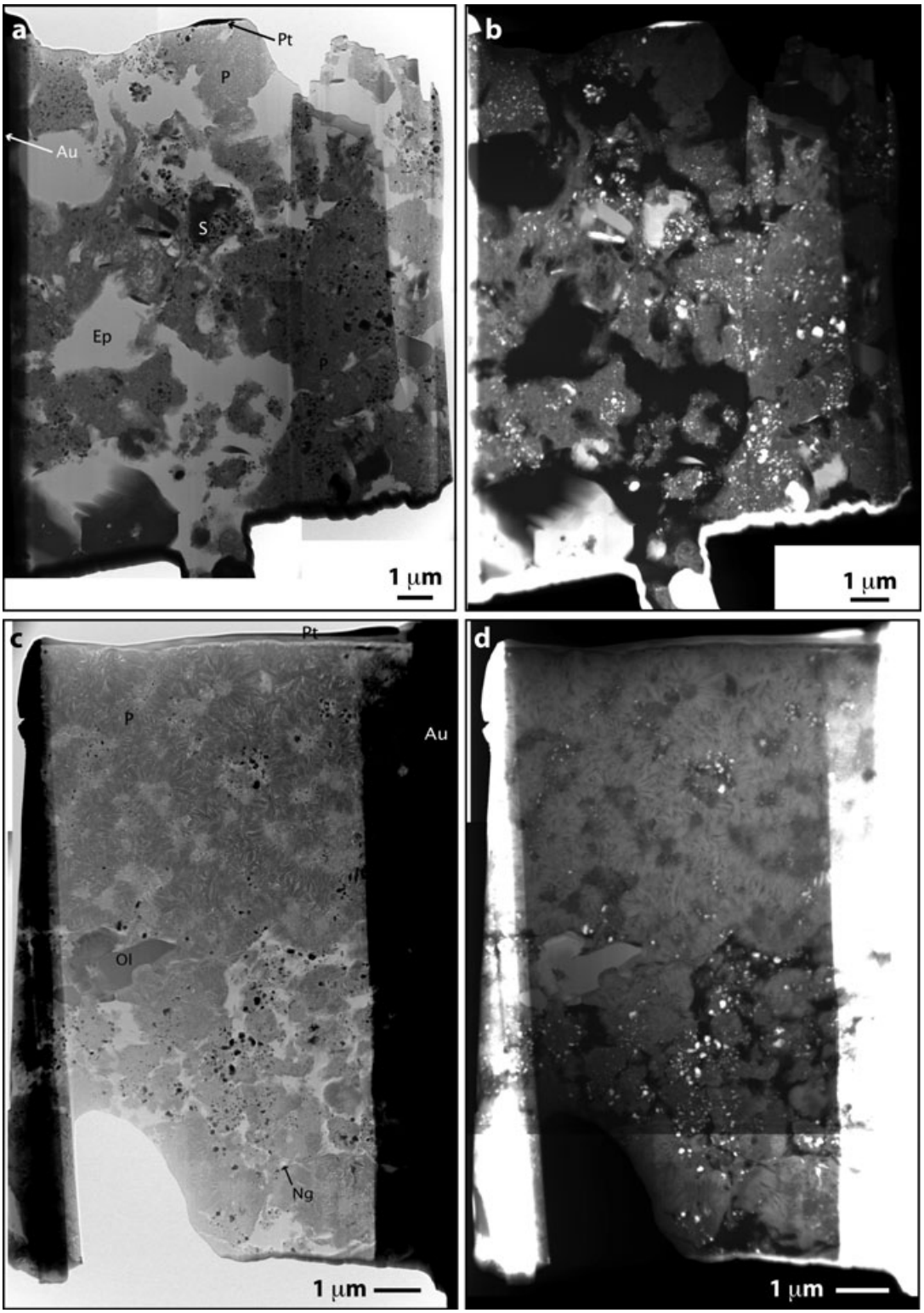

Fig. 11. Bright-field and HAADF-STEM images showing the FIB sections from TL11i. The FIB 11i-1 (a, b) was extracted from the part of the matrix that appears dark and porous on the macroscopic scale in BSE images, which is interpreted as a typical Tagish Lake matrix. FIB 11i-2 (c, d) was extracted from a lithic fragment, which is a more compact object with relatively higher contrast in BSE images. The lower part of this FIB section contains a fractured nanoglobule (black arrow). Pt = platinum; Au = gold; Ep = epoxy; S = sulfides; Ol = olivine; Ng = nanoglobule; P = phyllosilicates.

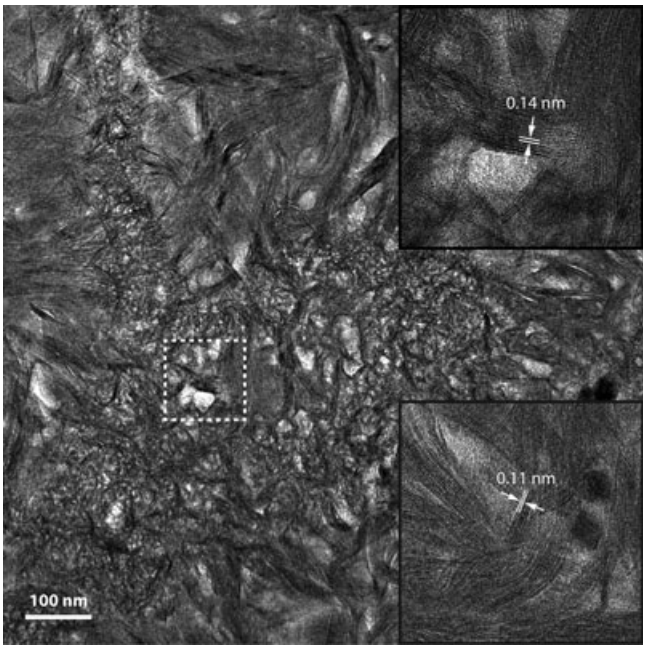

Fig. 12. HRTEM image of two TL11i FIB sections. Sheet silicates on this image, which is a part of the 11i-1 FIB section, exhibit sinuous textures with regions of coarse- and fine-grained sheet silicates that are intermixed with amorphous material in some areas. HRTEM measurements of both fine- and coarse-grained regions reveal an interlayered mixture of saponite (lattice-fringe spacings of approximately 0.11 nm) and chlorite-type phase (lattice-fringe spacings of 0.14 nm).

microstructure contain radial bundles with basal spacing of 0.9 nm, which more closely correspond to a smectite/saponite structure that tends to dehydrate under TEM vacuum causing a decrease in the layer spacing from 1.2 to 0.9 nm (Klimentidis and Mackinnon 1986). The lower part of this FIB section is enriched in sulfides and has a porous texture, similar to the FIB section of 11i-1. There is a large silicate grain on the boundary between the compact top and porous bottom areas of the section (white arrow on Fig. 11c). Part of the silicate grain (200 × 300 nm) is embayed on both sides by sheet silicates. A fractured nanoglobule, similar in appearance to the ones described by Nakamura et al. (2002), surrounded by fine-grained and ropy sheet silicates, occurs near the base of this FIB section (black arrow in Fig. 11c).

Specimen TL11h matrix

The bright-field and HAADF images (Figs. 10c and 10d) reveal an overall decrease in porosity across the 11h section. Some parts of it resemble the porosity of the TL5b matrix (top and bottom), whereas the middle is more compact. The sample contains abundant sulfides and carbonate grains. Some sulfides concentrate in large (2–3 × 0.5–1 μm) bands. The sulfide bands and carbonate grains are surrounded by sinuous sheet silicates. The middle part of the section is more compact and enriched in ribbon-like sheet silicates. Although this middle part is devoid of sulfide grains, a sulfide/oxide circular rim (possibly a highly altered chondrule) with a diameter of approximately 4–5 μm surrounds this more compact, sheet silicate–rich area. Within this area occurs a large (1 × 0.5 μm) grain identified through spectral imaging to be enriched in P, Ni, and Fe, possibly schreibersite, but the thickness of the grain precluded SAED. This P-bearing grain is locally embayed by sheet silicates, but otherwise completely surrounded by them. Several carbonate grains are present in this FIB section. Carbonate in the upper middle part of the section has a circular shape, and HAADF imaging shows concentric contrast variations. EDS spectral imaging indicates that the outside of this carbonate grain is enriched in Mg, Ca, and has minor Mn, whereas the core is enriched in Fe and sulfide grains (Fig. 14). Measurements from SAED patterns acquired from the core are consistent with a siderite structure.

DISCUSSION

Progressive Alteration

Chondrites in general preserve a complex record of different processes that occurred during the earliest stages of the solar system evolution. Many presolar and nebular processes have been obscured by later secondary asteroidal processes (Brearley 2004) particularly within highly altered chondritic groups such as CI and CM. The Tagish Lake meteorite has been classified as an ungrouped petrologic type 2 carbonaceous chondrite with affinities to both CI and CM, and has a mineralogy dominated by hydrated minerals, which suggests different stages of parent-body alteration (Zolensky et al. 2002).

Our mineralogic and petrologic observations indicate that there is a similarity in both primary (nebular-related) and secondary (alteration-related) components among the studied samples. This indicates that all four samples started off with similar anhydrous precursors; for example, all four samples initially had chondrules as primary components. Zolensky et al. (2002) noted an analogous observation for the Tagish Lake samples. However, the variation in component abundance in the studied four samples suggests an initial heterogeneity in the protolith material; for example, chondrules were heterogeneously distributed within the parent body. Furthermore, all samples experienced hydrous alteration that most likely occurred

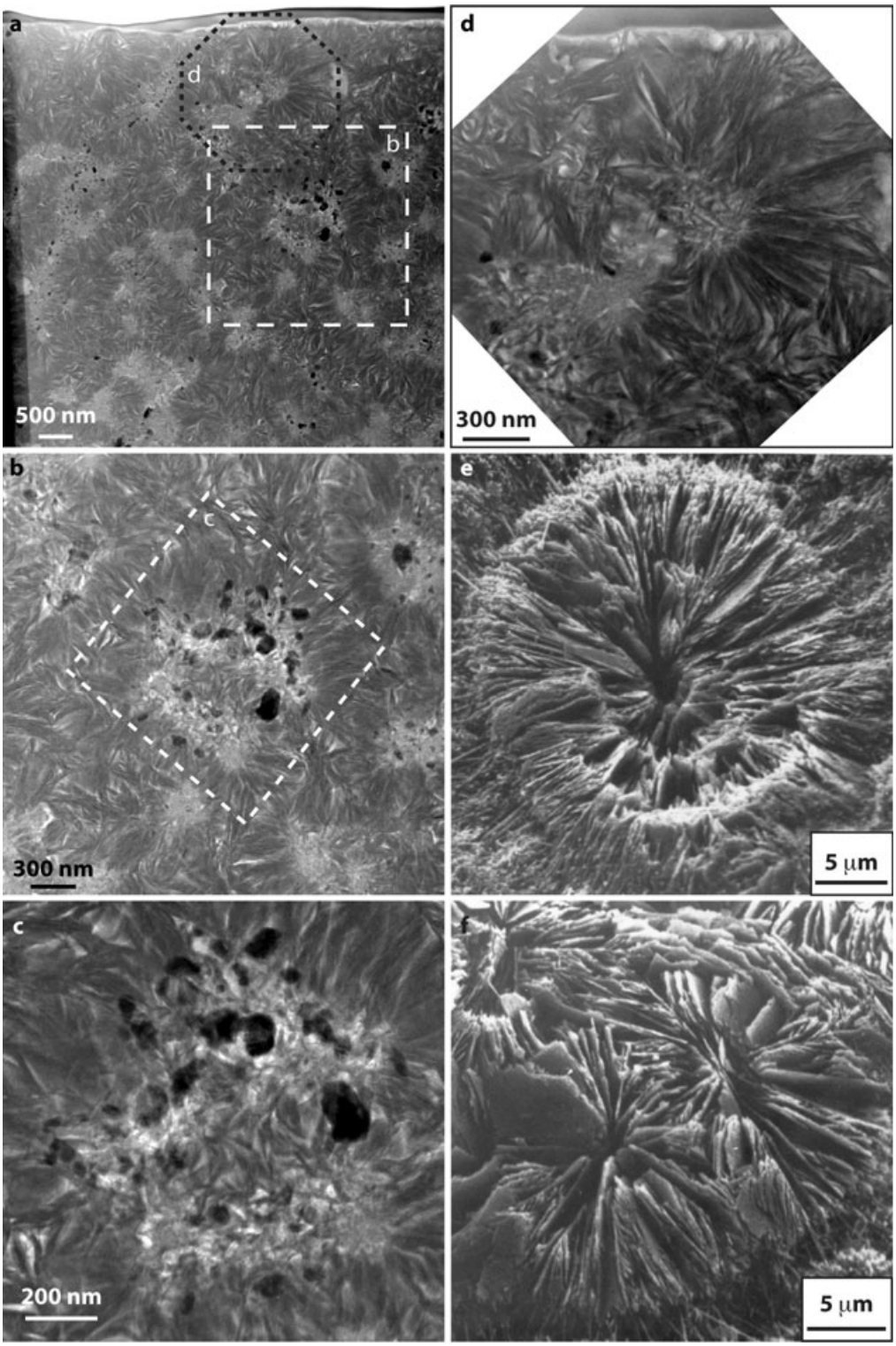

Fig. 13. a) TEM image of the top section of 11i-2 FIB section composed entirely of sheet silicates with a "flower"-like texture; b, c) close-up of the core consisting of sulfide/oxide grain and fine-grained sheet silicates with 0.7 nm basal spacing, consistent with serpentine structure; d) close-up of "flower"-like texture from the top of the section showing radial bundles radiating from the core having 0.9 nm basal spacings, consistent with smectite/saponite structure; e–f) SEM image of radial bundles of lizardite laths surrounded by fine-grained serpentine from terrestrial specimen 18515 (Cressey 1979; see text for detailed discussion). Reprinted with permission from *The Canadian Mineralogist*.

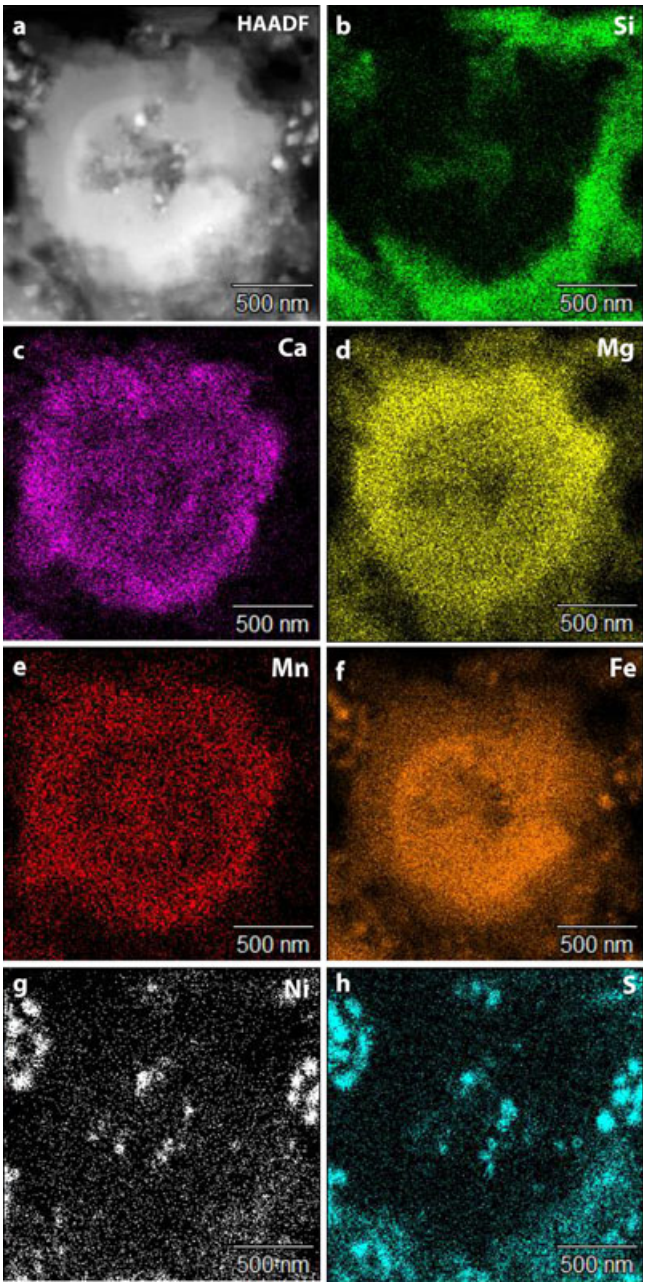

Fig. 14. STEM-EDS data on a carbonate grain from the TL11h FIB section. a) HAADF spectral image. b–h) STEM-based EDS maps. b) Si enrichment outside the grain (matrix). c, d, e) Respectively, Ca, Mg, and Mn enrichment in the shell. f) Fe enrichment in the core. g) Ni and (h) S enrichment spots in the core consistent with sulfides.

on the parent body as all primary nebular components, e.g., chondrules, have been altered. The intensity of such alteration was similar within each sample, but varied among the samples. Based on our observations, we infer that sample TL5b experienced less alteration compared with other samples because it contains unaltered silicate grains and devitrified mesostasis inside moderately altered chondrules. In comparison, both samples TL11v and TL11i have pseudomorphed chondrules, which are entirely replaced by sheet silicates, indicating a higher degree of alteration in these samples. Our observation of compact sheet silicate–rich lithic fragments, which are highly abundant in TL11i, also suggests that this lithology sampled a part of the protolith that experienced a higher water/rock ratio and some kind of brecciation. Thus, on the basis of petrologic and mineralogic observations, we conclude that the Tagish Lake parent body initially contained a heterogeneous mixture of anhydrous precursor minerals of nebular and presolar origin, which were later aqueously altered. The fragmentation of components, which could have happened before the incorporation into the final parent body (Takayama and Tomeoka 2012), and the degree of alteration were variable in different regions of the parent body. Palguda et al. (2010) showed that a nonuniform alteration is possible within a single protolith with a convecting hydrothermal system. Our data suggest that the studied samples recorded increasing degrees of alteration on the order of TL5b < TL11h < TL11i. Specimen TL11v, which consists of disaggregated material and is heterogeneous both on micro- and macroscale, encompasses the petrologic characteristics of the other three specimens as seen through EPMA observation.

This order of alteration is also supported by variations in organic matter and whole-rock oxygen data. Herd et al. (2011, 2012) showed that variations in organic matter, from the same four Tagish Lake samples studied here, correlate with variations in the inferred sequence of the parent-body aqueous alteration. These authors found that sample TL5b has a higher amount of more primitive insoluble organic matter (IOM) than sample TL11i, indicating more aqueous alteration effects on the latter sample. In addition, the IOM from the TL5b contains a higher fraction of nanoglobules than does the TL11v and TL11i IOM, indicating that the latter two samples have undergone higher degrees of hydrothermal alteration to preferentially destroy the isotopically anomalous nanoglobules. In other words, the alteration sequence recorded by the IOM reflects the observations from mineralogy and petrology with the least-altered TL5b to the more altered TL11v and TL11i.

This conclusion is also supported by the fact that the whole-rock oxygen-isotope analyses of the same four samples show that all fall on the same binary oxygen mixing isotopic trend (Herd et al. 2012). The least-altered sample TL5b is on one end of this trend closest to the CCAM (carbonaceous chondrite anhydrous mineral) line, while TL11i is on the other

end containing isotopically heavier sheet silicates, which are consistent with more extensive alteration (Herd et al. 2012). Therefore, both organics and whole-rock oxygen isotopes argue that these samples originated from the same material, or mixture of materials, and then were gradually hydrated to different degrees, in agreement with our mineralogic and petrologic results.

Formation of Sheet Silicates and the Origin of the Amorphous Material in TL5b

Our petrographic observations (both XRD and TEM) indicate a high volume of amorphous material in TL5b, suggesting that it is indigenous rather than a product of terrestrial weathering. Amorphous material has been found both in the FGRs and the matrices of CM and CR chondrites (e.g., Chizmadia and Brearley 2008; Abreu and Brearley 2010). Detailed petrographic studies of the rims in CM chondrites (e.g., Y-791198) indicate the presence of abundant amorphous material intermixed with nanocrystalline phyllosilicates consistent with limited thermally driven growth (Chizmadia and Brearley 2008). Matrices dominated by amorphous material were also found in two primitive, low metamorphic grade, CR chondrites (MET00426 and QUE99177), suggesting that thermal metamorphism and low-temperature parent-body alteration did not occur or was minimal (Abreu and Brearley 2010).

In our TEM observations of TL5b, we see abundant amorphous material with rare bundles of fine-grained sheet silicates, comparable to the microstructure, found in the FGRs and matrices of CM and CR chondrites. We conclude that TL5b underwent lower T hydrothermal alteration or experienced lower water/rock than other studied samples (TL11i, TL11h) to preserve the observed amorphous material and produce fine-grained sheet silicates. Herd et al. (2011) inferred an upper limit for the Tagish Lake protolith alteration of approximately 150 °C to preserve volatile organic compounds seen in these samples. Our petrographic observations of the amorphous material in the TL5b suggest that this sample experienced temperatures of ≤50 °C. Progressive alteration of the metastable amorphous material results in the formation of increasingly coarse sheet silicates with continued alteration (Jones and Brearley 2006; Brearley and Burger 2006). The limited amount of amorphous material in the other studied Tagish Lake samples argues that they were affected by either longer alteration at higher T (>150 °C) or higher water/rock ratio to preferentially destroy the amorphous material in favor of fine- and coarse-grained sheet silicates (Chizmadia and Brearley 2008; Brearley and Burger 2009).

There are several hypotheses for the origins of amorphous material. Theories for its formation include: shock metamorphism, weathering of FeO-rich olivines, alteration of nebular material, or surviving nonequilibrium condensate from the solar nebula (Day and Donn 1978; Nuth and Donn 1983; Brearley 1993; Greshake 1997; Chizmadia and Brearley 2008; Abreu and Brearley 2010; Keller and Messenger 2011). The production of amorphous material by shock metamorphism does not fit with the observed petrography of TL5b. The shock-induced structures, such as high-density dislocations, planar fractures, and deformations (Greshake 1997), have not been observed in any Tagish Lake samples in this study. It was also noted that such shock processing would deplete the matrix in dissolved S and produce globules of sulfides (Ashworth 1985). In comparison, we find that the matrix in all four samples is highly enriched in S and Ni, and the morphology of sulfides is not globular (Fig. 8). The data are also not consistent with a formation via alteration of the FeO-rich olivines. The product of such alteration would be highly heterogeneous intergrowths or wispy grains of Fe-oxide and silicate (Jones and Brearley 2006; Chizmadia and Brearley 2008), and we have not observed such morphologies in TL5b or the other samples studied herein. We cannot completely rule out parent-body hydrous alteration as a possible origin of amorphous material in the Tagish Lake meteorite as recent observations of some CR chondrites show that amorphous material in those meteorites is hydrated (Le Guillou et al. 2013). Therefore, it is possible that some amorphous material found in Tagish Lake samples is also hydrated. However, the fact that we observed the highest amount of amorphous material in the least-altered sample (TL5b) is a strong indicator that hydrous alteration is not the dominant formation mechanism. In addition, the sample TL11i, which showed the greatest levels of aqueous alteration, is dominated by coarse-grained sheet silicates not amorphous silicates. On the basis of the above arguments, we infer that most of the amorphous material found in TL5b is of nebular origin similar to that in some CM, CO, and CR chondrites (e.g., Brearley 1993; Chizmadia and Brearley 2008; Abreu and Brearley 2010).

Although some of the amorphous silicates are likely nebular in origin, some may be presolar (e.g., Chizmadia and Brearley 2008). Brown et al. (2000) first indicated the presence of presolar grains in the Tagish Lake meteorite. This was later supported by Nakamura et al. (2003) who observed high levels of primordial noble gas indicative of high concentrations of presolar diamonds and SiC/graphite grains. Marhas and Hoppe (2005) reported 4 ppm presolar silicates within a Tagish

Lake thin section of unknown alteration grade, an abundance that is small compared with primitive meteorites (up to 200 ppm) and the most primitive IDPs (>400 ppm). We have not yet measured the presolar silicate abundance in our samples, but on the basis of the variation in degree of alteration and abundance of amorphous material, we expect that if presolar silicates are preserved, then TL5b should contain higher quantities than TL11h and TL11i.

Formation of Sulfides

Exsolved pentlandite in pyrrhotite has been previously reported in other carbonaceous chondrites such as CI, CM, and CR (e.g., Fuchs et al. 1973; Ramdohr 1973; Brearley and Martinez 2010; Schrader et al. 2010), and nonexsolved pentlandite along grain boundaries has been observed in several hydrated IDPs (Tomeoka and Buseck 1984; Zolensky and Thomas 1995). The studied specimens contain a large number of sulfides of intermediate composition, and in BSE images, we encounter grains with both exsolved and nonexsolved morphologies (Fig. 8). Our observations of exsolved pentlandite from pyrrhotite in our samples (Figs. 8a–d) are contrary to Boctor et al. (2003) who did not observe any exsolution in Fe-Ni monosulfide solid solution (MSS) in Tagish Lake meteorite. The exsolved sulfide morphologies that we observe in our samples are similar to those reported by Lauretta et al. (1997) for pentlandite synthesized via gas-solid reactions under nebular conditions suggesting that at least some of the Tagish Lake exsolved sulfides formed at higher temperatures in a nebular environment. In comparison, some exsolved pentlandite, e.g., the "flame" texture, could possibly be a product of metal diffusion from Ni-bearing MSS during cooling in the solar nebula at temperatures <600 °C over extended periods of time (approximately 3000–30,000 years) (Brearley and Martinez 2010).

It was reported that pentlandite can also form at lower temperatures (≤200 °C) or more rapid cooling, forming nonexsolved granular pentlandite at interstices between grains and along grain boundaries (Durazzo and Taylor 1982; Vaughan and Craig 1997). Nonexsolved pentlandite has also been observed as a product of high oxygen fugacity conditions during aqueous alteration (Godlevskiy et al. 1971), which is thought to be consistent with conditions of nonexsolved pentlandite observed in hydrous IDPs (Zolensky and Thomas 1995). Comparison of morphologies in our samples with those previously reported suggests that pentlandite found along the pyrrhotite grain boundaries is a product of aqueous alteration on the parent body. Similarly, the "bull's-eye" morphology consisting of a core and rim separated by a gap (Figs. 8e and 8f) and sulfide rims found around highly altered chondrules (Figs. 7c and 7d) possibly fall into the same generation of sulfides, which were formed by multiple precipitation episodes during low-temperature alteration (≤100 °C) (Zolensky et al. 2002).

Formation of the "Flower"-like Microstructure in the Lithic Fragment

To our knowledge, the coronal, "flower"-like serpentine microstructure observed in the FIB section of lithic fragment TL11i (Fig. 13) has not been reported in other chondrites. The closest forms are polygonal serpentine reported by Zega et al. (2003, 2004, 2006) in CM chondrites. These structures contain polygonal sectors formed by concentric lizardite layers with periodic inversion of the tetrahedral sheet, resulting in kinked layers wrapped around a tube axis. The kinking is due to the structural mismatch between the tetrahedral silica sheet and the octahedral Mg-bearing sheet (e.g., Dódony 1997). Such structures were inferred to have formed through intense alteration under oxidizing conditions (Zega et al. 2004, 2006). The "flower"-like textures that we observe in Tagish Lake, while exhibiting a round morphology similar to polygonal forms, do not show polygonal geometry and appear to be of a different nature than those described by Zega et al. (2004, 2006).

Cressey (1979) reported radial structures in vein margins in serpentinized peridotite from the Lizard, Cornwall, England (Figs. 13e and 13f), and described these objects as consisting of radial bundles or blades of lizardite laths surrounded by fine-grained serpentine with no apparent core. These authors also noted that although these structures closely resemble spherulites in polymers, they are cylindrical, not spherical, in three dimensions. Cressey (1979) postulated that observed terrestrial lizardite structures probably formed under unique conditions in a hydrothermal vein. The formation was probably facilitated by high nucleation and growth rates producing skeletal-type structures followed by a rapid quenching similar to conditions in the chilled margins of a basic intrusion (Cressey 1979). In comparison, these terrestrial textures, although similar at first glance to those we observe in the Tagish Lake meteorite, differ in mineralogy and overall geometry, i.e., the terrestrial forms appear to lack distinct cores (Cressey 1979). We cannot infer from the data at hand whether the observed radial structures in TL11i have a spherical or cylindrical three-dimensional space. However, based on lattice-fringe measurements of localized areas within the structure, the cores contain serpentine and the radial bundles consist of a

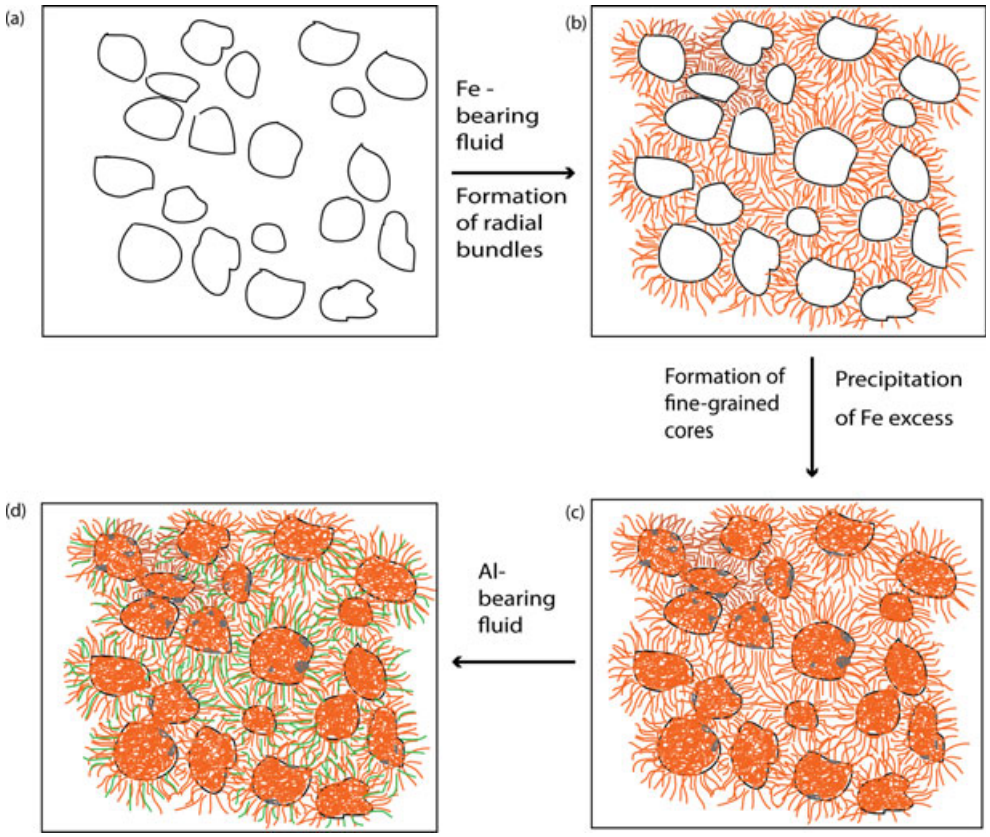

Fig. 15. Schematic representation of the model for the formation of the "flower"-like textures of 11i-2 FIB section, found within the lithic fragment (see text for details). a) Precursor loosely packed clusters of anhydrous semirounded silicate grains (a few microns in diameter) were subjected to alteration from the outside. b) Clusters were subjected to Fe-bearing fluids, which percolated through the cracks/pore space between and around these semirounded grains. Serpentine formed in this space in a radial fashion. The radial arrays had more time to crystallize to form coarse-grain morphology. c) The fluids then proceeded to alter the semirounded grains to produce fine-grained cores of the future "flower"-like textures. Any excess was precipitated as sulfides and/or magnetite. d) Introduction of Al-bearing fluid percolated through the bundles, which produced a mixture of serpentine-saponite. Colors: orange—serpentine precipitation from Fe-bearing fluids; gray—excess Fe precipitated as sulfides and/or magnetite; green—saponite precipitated from Al-bearing fluid.

combination of serpentine and saponite. We hypothesize that pore space played a role in producing the radial bundles observed in the coronal, "flower"-like texture in TL11i.

It is widely accepted that hydrous processing of asteroidal bodies occurred after accretion (Brearley and Jones 1998; Brearley 2004), and that the hydration process varied in duration and chemistry. For example, there are local regions within the studied Tagish Lake samples where alteration appears to have been nearly complete, e.g., the embayment in the phosphate grain in TL11h (Fig. 10c) and partially altered silicate grain at the boundary of the top and bottom portions of TL11i-2 (Fig. 11c). These observations suggest a possible intermittent availability of fluids or the permeability of the matrix to allow fluids to penetrate into some areas of the grain more readily than others. In other areas, the mineralogy suggests variation in fluid composition, e.g., change in carbonate grain composition from Fe-rich to more Mg-rich (Fig. 14). In addition, the presence of both fine-grained and coarse-grained textures observed in the sheet silicates (Fig. 12) likely represents thermally driven recrystallization fronts (Jones and Brearley 2006; Brearley and Burger 2006). The coronal, "flower"-like textures in TL11i-2 show both compositional (saponite and serpentine mixture in the radial arrays, and serpentine only in the core) and textural (fine-grained in the core, and coarse-grained in the arrays) changes (Fig. 13). We suspect that these textures formed as a result of different pulses of fluids with changing composition and varying duration.

We hypothesize that loosely packed clusters of anhydrous, semirounded silicate grains (a few microns in diameter) were subjected to alteration from the outside (Fig. 15a). At first, these clusters were

subjected to Fe-bearing fluids, which percolated through the cracks/pore space between and around these semirounded grains. Serpentine formed in this space in a radial fashion (Fig. 15b) similar to a terrestrial hydrothermal vein environment (e.g., Cressey 1979). The radial arrays had more time to crystallize to form a coarse-grained morphology. The fluids then proceeded to alter the semirounded grains to produce fine-grained cores of the future "flower"-like textures (Fig. 15c). Any excess Fe was precipitated as sulfides and/or magnetite found in and around the cores of these structures (Fig. 15c). The last stage of the alteration is late introduction of Al-bearing fluid to alter the radial arrays only to produce a mixture of serpentine-saponite that we observe (Fig. 15d).

An alternative hypothesis is that the "flower"-like textures were produced by altering the grains first to generate the cores followed by the growth of radial bundles into the pore spaces. Although hydrothermal experiments depicting the models' conditions are necessary to determine the formation stages of such texture, the fact that we observe similar "flower"-like textures in the altered chondrule of TL11h (Fig. 7c) is consistent with our first preferred hypothesis. This chondrule was subjected to alteration fluids that appear to have percolated through the cracks between the olivine grains to produce radial bundles in the cracks, followed by alteration of the grains to produce fine-grained cores in a similar fashion to our proposed model. The altered chondrule in Fig. 7a is also consistent with our proposed model. This chondrule preserves a snapshot of the alteration in progress showing serpentine radial arrays growing around partially altered olivine grains (Fig. 7b).

CONCLUSIONS

1. On the basis of petrologic and mineralogic observations, we conclude that the Tagish Lake parent body consisted of a heterogeneous mixture of anhydrous precursors of nebular origin, which were fragmented prior to accretion. The same material was subsequently aqueously altered to varied degrees on the parent body. The degree to which the studied samples experienced aqueous alteration is in the order TL5b < TL11h < TL11i. Specimen TL11v, which consists of disaggregated material, is heterogeneous on the microscale and encompasses the petrologic characteristics of other three specimens as seen through EPMA observation. This conclusion is also supported by variations in organic matter and whole-rock oxygen data (Herd et al. 2011, 2012).
2. The presence of the abundant amorphous material in the TL5b argues that this sample experienced relatively milder parent-body alteration to preserve this indigenous nebular material and produce fine-grained sheet silicates. Other samples were subjected to a longer duration of hydrous alteration, or higher fluid/rock ratio, as they are dominated by coarse-grained sheet silicates.
3. We observed two generations of sulfides in the studied samples. The first generation consists of exsolved pentlandite morphologies, which formed at higher temperature in the cooling solar nebula or via metal diffusion from Ni-bearing MSS during cooling of the solar nebula below temperatures < 600 °C. The second generation includes nonexsolved pentlandite along grain boundaries, the "bull's-eye" sulfide morphology, and rims around highly altered chondrules, which all formed by multiple precipitation episodes during low-temperature aqueous alteration (≤ 100 °C) on the parent body.
4. The coronal, "flower"-like microtexture consisting of core and radial arrays, observed in a lithic fragment from sample TL11i, shows both compositional changes from serpentine in the core to saponite-serpentine in the radial arrays and textural changes from fine-grained in the core to coarse-grained in the arrays. Our preferred model for production of this texture involves serpentine precipitation in the pore spaces around silicate grains to produce coarse-grained radial arrays, subsequent alteration of silicate grains to form fine-grained cores, and later introduction of Al-bearing fluid to precipitate the saponite in the already serpentinized cracks.

Acknowledgments—We thank the following people from the Department of Earth and Atmospheric Sciences, University of Alberta, who helped us with various stages of this project: Sergei Matveev helped with EPMA; Diane Caird and Andrew Locock helped with XRD. AB thank Fred Wicks, and Barbara and Gordon Cressey for in-depth discussions on the nature of serpentines. The authors thank Emma Bullock for helping with SEM. Travel to the Naval Research Laboratory, Washington, D.C., was generously supported by the Carnegie Institution of Canada grant to Larry Nittler. This project was supported by the following organizations: NASA Astrobiology grant to Carnegie Institution of Washington; NASA Origins and Cosmochemistry grants to TJZ and RMS; Natural Sciences and Engineering Research Council (NSERC) of Canada grant to CDKH; and CGS D3 NSERC, the Alberta Ingenuity doctoral scholarships and Dissertation Fellowship to AB. We thank Adrian Brearley, Lysa Chizmadia, and Mike Zolensky for their

detailed reviews of the original manuscript, which resulted in a much improved final version on this paper.

Editorial Handling—Dr. Adrian Brearley

REFERENCES

Abreu N. M. and Brearley A. J. 2010. Early solar system processes recorded in the matrices of two highly pristine CR3 carbonaceous chondrites, MET 00426 and QUE 99177. *Geochimica et Cosmochimica Acta* 74:1146–1171.

Ashworth J. R. 1985. Transmission electron-microscopy of L-group chondrites. 1. Natural shock effects. *Earth and Planetary Science Letters* 73:17–32.

Baker L., Franchi I. A., Wright I. P., and Pillinger C. T. 2002. The oxygen isotopic composition of water from Tagish Lake: Its relationship to low-temperature phases and to other carbonaceous chondrites. *Meteoritics & Planetary Science* 37:977–985.

Benedix G. K., Leshin L. A., Farquhar J., Jackson T., and Thiemens M. H. 2003. Carbonates in CM2 chondrites: Constraints on alteration conditions from oxygen isotopic compositions and petrographic observations. *Geochimica et Cosmochimica Acta* 67:1577–1588.

Bland P. A., Cressey G., and Menzies O. N. 2004. Modal mineralogy of carbonaceous chondrites by X-ray diffraction and Mossbauer spectroscopy. *Meteoritics & Planetary Science* 30:3–16.

Blinova A., Herd C. D. K., Zega T., De Gregorio B., and Stroud R. 2009. Preliminary SEM and TEM study of pristine samples of Tagish Lake Meteorite (abstract #2039). 40th Lunar and Planetary Science Conference. CD-ROM.

Blinova A., Zega T., Herd C. D. K., and Stroud R. 2011. A TEM study of the pristine matrix from the Tagish Lake meteorite (abstract #2517). 42nd Lunar and Planetary Science Conference. CD-ROM.

Blinova A., Alexander C. M. O'D., Wang J., and Herd C. D. K. 2012. Mineralogy and Mn-Cr extinct radionuclide dating of a dolomite from the pristine Tagish Lake Meteorite (abstract #1188). 43rd Lunar and Planetary Science Conference. CD-ROM.

Boctor N. Z., Kurat G., and Alexander C. M. O'D. 2003. Sulfide-oxide assemblage in Tagish Lake carbonaceous chondrite (abstract #1705). 34th Lunar and PLanetary Science. CD-ROM.

Brandelik A. 2009. CALCMIN—an EXCEL Visual Basic application for calculating mineral structural formulae from electron microprobe analyses. *Computers and Geosciences* 35:1540–1551.

Brearley A. J. 1993. Matrix and fine-grained rims in the unequilibrated CO3 chondrite, ALHA77307: Origins and evidence for diverse, primitive nebular dust components. *Geochimica et Cosmochimica Acta* 57:1521–1550.

Brearley A. J. 2004. Nebular versus parent-body processing. In *Treatise on geochemistry*, edited by Davis A. M. Oxford: Elsevier Ltd. pp. 247–268.

Brearley A. J. and Burger P. V. 2006. Experimental hydrothermal alteration of Kainsaz (CO3) under anoxic conditions: Constraints on aqueous alteration in carbonaceous chondrites. *Meteoritics & Planetary Science* 41:A28.

Brearley A. J. and Burger P. V. 2009. Mechanisms of aqueous alteration of type IIA chondrule glass in the CR chondrite EET 92105: Insights from FIB/TEM analysis. *Meteoritics & Planetary Science* 44:A39.

Brearley A. J. and Jones R. H. 1998. Chondritic meteorites. In *Planetary materials*, edited by Papike J. J. Washington, D.C.: Mineralogical Society of America. pp. 3-1–3-398.

Brearley A. J. and Martinez C. 2010. Ubiquitous exsolution of pentlandite and troilite in pyrrhotite from the TIL 91722 CM2 carbonaceous chondrite: A record of low temperature solid state processes (abstract #1689). 41st Lunar and Planetary Science Conference. CD-ROM.

Brown P. G., Hildebrand A. R., Zolensky M. E., Grady M., Clayton R. N., Mayeda T. K., Tagliaferri E., Spalding R., MacRae N. D., Hoffman E. L., Mittlefehldt D. W., Wacker J. F., Bird J. A., Campbell M. D., Carpenter R., Gingerich H., Glatiotis M., Greiner E., Mazur M. J., and McCausland P. J. A. 2000. The fall, recovery, orbit, and composition of the Tagish Lake Meteorite: A new type of carbonaceous chondrite. *Science* 290:320–325.

Brown P. G., ReVelle D. O., Tagliaferri E., and Hildebrand A. R. 2002. An entry model for the Tagish Lake fireball using seismic, satellite and infrasound records. *Meteoritics & Planetary Science* 37:661–675.

Browning L. B., McSween H. Y., and Zolensky M. E. 1996. Correlated alteration effects in CM carbonaceous chondrites. *Geochimica et Cosmochimica Acta* 60:2621–2633.

Bullock E. S., Grady M. M., Russell S. S., and Gounelle M. 2005. Fe-Ni sulphides within a CM1 clast in Tagish Lake (abstract #1883). 36th Lunar and Planetary Science Conference. CD-ROM.

Chizmadia L. and Brearley A. J. 2008. Mineralogy, aqueous alteration, and primitive textural characteristics of fine-grained rims in the Y-791198 CM2 carbonaceous chondrite: TEM observations and comparison to ALHA81002. *Geochimica et Cosmochimica Acta* 72:602–625.

Cressey B. A. 1979. Electron microscopy of serpentinite textures. *Canadian Mineralogist* 17:741–756.

David W. I. F. 2004. Power diffraction: Least-squares and beyond. *Journal of Research of the National Institute of Standards and Technology* 109(1):107–123.

Day K. L. and Donn B. 1978. Condensation of non-equilibrium phases of refractory silicates from vapor. *Science* 202:307–308.

Dódony I. 1997. Structure of the 30-sector polygonal serpentine: A model based on TEM and SAED studies. *Minerals Physics and Chemistry of Minerals* 24:39–49.

Droop G. T. R. 1987. A general equation for estimating Fe3 + concentrations in ferromagnesian silicates and oxides from microprobe analyses, using ctoichiometric criteria. *Mineralogical Magazine* 51:431–435.

Durazzo A. and Taylor L. A. 1982. Exsolution in the MSS-pentlandite system—Textural and genetic implications for Ni-sulfide ores. *Mineralium Deposita* 17:313–332.

Endress M. and Bischoff A. 1996. Carbonates in CI chondrites: Clues to parent body alteration. *Geochimica et Cosmochimica Acta* 60(3):489–507.

Fuchs L. H., Olsen E. J., and Gebert E. 1973. New x-ray and compositional data for farringtonite, $Mg_3(PO_4)_2$. *American Mineralogist* 58:949–951.

Godlevskiy M. N., Likhachev A. P., Chuvkin N. G., and Andronov A. D. 1971. Geothermal synthesis of

pentlandite. *Dokldy Akademii Nauk USSR* 196(5):1182–1185.

Greshake A. 1997. The primitive matrix components of the unique carbonaceous chondrite Acfer 094: A TEM study. *Geochimica et Cosmochimica Acta* 61:437–452.

Greshake A., Krot A. N., Flynn G. J., and Keil K. 2005. Fine-grained dust rims in the Tagish Lake carbonaceous chondrite: Evidence for parent body alteration. *Meteoritics & Planetary Science* 40:1413–1431.

Hanowski N. P. and Brearley A. J. 2000. Iron-rich aureoles in the CM carbonaceous chondrites Murray, Murchison, and Allan Hills 81002: Evidence for in situ aqueous alteration. *Meteoritics & Planetary Science* 35:1291–1308.

Hanowski N. P. and Brearley A. J. 2001. Aqueous alteration of chondrules in the CM carbonaceous chondrite, Allan Hills 81002: Implications for parent body alteration. *Geochimica et Cosmochimica Acta* 65:495–518.

Herd R. K., and Herd C. D. K. 2007. Towards systematic study of the Tagish Lake meteorite (abstract #2347). 38th Lunar and Planetary Science Conference. CD-ROM.

Herd C. D. K., Blinova A., Simkus D. N., Huang Y., Tarozo R., Alexander C. M. O'D., Gyngard F., Nittler L. R., Cody G. D., Fogel M. L., Kebukawa Y., Kilcoyne A. L. D., Hilts R. W., Slater G. F., Glavin D. P., Dworkin J. P., Callahan M. P., Elsila J. E., De Gregorio B. T., and Stroud R. M. 2011. Origin and evolution of prebiotic organic matter as inferred from the Tagish Lake Meteorite. *Science* 332:1304–1307.

Herd C. D. K., Sharp Z. D., Alexander C. M. O'D., and Blinova A. 2012. Oxygen isotopic composition of Tagish Lake lithologies: Insights into parent body alteration (absract #1688). 43rd Lunar and Planetary Science Conference. CD-ROM.

Hildebrand A. R., McCausland P. J. A., Brown P. G., Longstaffe F. J., Russell S. S., Tagliaferri E., Wacker J. F., and Mazur M. J. 2006. The fall and recovery of the Tagish Lake meteorite. *Meteoritics & Planetary Science* 41:407–431.

Howard K. T., Benedix G. K., Bland P. A., and Cressey G. 2009. Modal mineralogy of CM2 chondrites by X-ray diffraction (PSD-XRD). Part 1. Total phyllosilicate abundance and the degree of aqueous alteration. *Geochimica et Cosmochimica Acta* 73:4576–4589.

Howard K. T., Benedix G. K., Bland P. A., and Cressey G. 2011. Modal mineralogy of CM2 chondrites by X-ray diffraction (PSD-XRD). Part 2. Degree, nature and settings of aqueous alteration. *Geochimica et Cosmochimica Acta* 75:2735–2751.

Izawa M. R. M., Flemming R. L., King P. L., Peterson R. C., and McCausland P. J. A. 2010. Mineralogical and spectroscopic investigation of the Tagish Lake carbonaceous chondrite by X-ray diffraction and infrared reflectance spectroscopy. *Meteoritics & Planetary Science* 45:675–698.

Jarosewich E. 2002. Smithsonian Microbeam Standards. *Journal of Research National Institute of Standards and Technology* 107:681–685.

Jones C. L. and Brearley A. J. 2006. Experimental aqueous alteration of the Allende meteorite under oxidizing conditions: Constraints on asteroidal alteration. *Geochimica et Cosmochimica Acta* 70:1040–1058.

Keller L. P. and Messenger S. 2011. On the origins of GEMS grains. *Geochimica et Cosmochimica Acta* 75: 5336–5365.

Kerridge J. F. 1970. Some observations on the nature of magnetite in the Orgueil meteorite. *Earth and Planetary Science Letters* 9:299–306.

Klimentidis R. E. and Mackinnon I. D. R. 1986. High-resolution imaging of ordered mixed-layer clays. *Clays and Clay Minerals* 34:155–164.

Kminek G., Botta O., Glavin D. P., and Bada J. L. 2002. Amino acids in the Tagish Lake meteorite. *Meteoritics & Planetary Science* 37:697–701.

Lauretta D. S., Lodders K., and Fegley B. Jr. 1997. Experimental simulations of sulfide formation in the solar nebula. *Science* 277:358–360.

Le Guillou C., Remusat L., Bernard S., Brearley A. J., and Hugues L. 2013. Amorphization and D/H fractionation of kerogens during experimental electron irradiation; comparison with chondritic organic matter. *Icarus* 226:101–110.

Marhas K. K. and Hoppe P. 2005. Presolar grains in the Tagish Lake meteorite. *Meteoritics & Planetary Science* 40: A95.

McSween H. Y. Jr. 1977. Carbonaceous chondrites of the Ornans type: A metamorphic sequence. *Geochimica et Cosmochimica Acta* 44:477–491.

Metzler K., Bischoff A., and Stōffler D. 1992. Accretionary dust mantles in CM chondrites: Evidence for solar nebula processes. *Geochimica et Cosmochimica Acta* 56:2873–2897.

Nakamura K., Zolensky M. E., Tomita S., Nakashima S., and Tomeoka K. 2002. Hollow organic globules in the Tagish Lake meteorite as possible products of primitive organic reactions. *International Journal of Astrobiology* 1:179–189.

Nakamura T., Noguchi T., Zolensky M. E., and Tanaka M. 2003. Mineralogy and noble-gas signatures of the carbonate-rich lithology of the Tagish Lake carbonaceous chondrite: Evidence for an accretionary breccia. *Earth and Planetary Science Letters* 207:83–101.

Nuth J. A. and Donn B. 1983. Laboratory studies of the condensation and properties of amorphous silicate smokes. *Journal of Geophysical Research* 88:A847–A852.

Palguda J., Schubert G., and Travis B. J. 2010. Fluid flow and chemical alteration in carbonaceous chondrite parent bodies. *Earth and Planetary Science Letters* 296:235–243.

Petitat M., Birck J.-L., Luu T. H., and Gounelle M. 2011. The chromium isotopic composition of the ungrouped carbonaceous chondrite Tagish Lake. *The Astrophysical Journal* 736:23.

Ramdohr P. 1973. *The opaque minerals in stony meteorites*. New York: Elsevier Publishing Company, 245 p.

Russell S. D. J., Longstaffe F. J., King P. L., and Larson T. E. 2008. Whole-rock, clay mineral, and olivine oxygen and hydrogen isotope compositions of the Tagish Lake carbonaceous chondrite (abstract #1709). 39th Lunar and Planetary Science Conference. CD-ROM.

Schrader D. L., Connolly H. C. Jr., and Lauretta D. S. 2010. On the nebular and aqueous signatures in the CR chondrites (abstract# 1262). 41st Lunar and Planetary Science Conference. CD-ROM.

Simon S. B. and Grossman L. 2003. Petrography and mineral chemistry of the anhydrous component of the Tagish Lake carbonaceous chondrite. *Meteoritics & Planetary Science* 38:813–825.

Takayama A. and Tomeoka K. 2012. Fine-grained rims surrounding chondrules in the Tagish Lake carbonaceous

chondrite: Verification of their formation through parent-body processes. *Geochimica et Cosmochimica Acta* 98:1–18.

Tomeoka K. and Buseck P. R. 1984. Transmission electron-microscopy of the low-Ca hydrated interplanetary dust particle. *Earth and Planetary Science Letters* 69:243–254.

Tomeoka K. and Buseck P. R. 1988. Matrix mineralogy of the Orgueil CI carbonaceous chondrite. *Geochimica et Cosmochimica Acta* 52:1627–1640.

Vaughan D. J. and Craig J. R. 1997. Sulfide ore mineral stabilities, morphologies, and intergrowth textures. In *Geochemistry of hydrothermal ore deposits*, 3rd ed., edited by Barnes H. L. New York: John Wiley and Sons, Inc. pp. 367–434.

Weisberg M. and Huber H. 2007. The GRO95577 CR1 chondrite and hydration of the CR parent body. *Meteoritics & Planetary Science* 42:1495–1503.

Weisberg M., Prinz M., Clayton R. N., and Mayeda T. K. 1993. The CR (Renazzo-type) carbonaceous chondrite group and its implications. *Geochimica et Cosmochimica Acta* 57:1567–1586.

Zega T. J., Garvie L. A. J., and Buseck P. R. 2003. Nanometer-scale measurements of iron oxidation states of cronstedtite from primitive meteorites. *American Mineralogist* 88:1169–1172.

Zega T. J., Garvie L. A. J., Dódony I., and Buseck P. R. 2004. Serpentine nanotubes in the mighei CM chondrite. *Earth and Planetary Science Letters* 223:141–146.

Zega T. J., Garvie L. A. J., Dódony I., Friedrich H., Stroud R. M., and Buseck P. R. 2006. Polyhedral serpentine grains in CM chondrites. *Meteoritics & Planetary Science* 41:681–688.

Zega T. J., Nittler L. R., Busemann H., Hoppe P., and Stroud R. M. 2007. Coordinated isotopic and mineralogic analyses of planetary materials enabled by in situ lift-out with a focused ion beam scanning electron microscope. *Meteoritics & Planetary Science* 42:1373–1386.

Zega T. J., Alexander C. M. O'D., Busemann H., Nittler L. R., Hoppe P., Stroud R. M., and Young A. F. 2010. Mineral associations and character of isotopically anomalous organic material in the Tagish Lake carbonaceous chondrite. *Geochimica et Cosmochimica Acta* 74:5966–5983.

Zolensky M. E. and Thomas K. L. 1995. Iron and iron-nickel sulfides in chondritic interplanetary dust particles. *Geochimica et Cosmochimica Acta* 59:4707–4712.

Zolensky M., Barrett R., and Browning L. 1993. Mineralogy and composition of matrix and chondrule rims in carbonaceous chondrites. *Geochimica et Cosmochimica Acta* 57:3123–3148.

Zolensky M. E., Nakamura K., Gounelle M., Mikouchi T., Kasama T., Tachikawa O., and Tonui E. 2002. Mineralogy of Tagish Lake: An ungrouped type 2 carbonaceous chondrite. *Meteoritics & Planetary Science* 37:737–761.